J. Webster (ed.), *Wiley Encyclopedia of Electrical and Electronics Engineering*

RADAR CROSS-SECTION

Radar cross-section (*RCS*) is a measure of the magnitude of the scattered electromagnetic wave from a body relative to the magnitude of the wave incident on the body. To many people RCS is synonymous with stealth. Stealth technology has become an integral part of all military systems since it was first employed in the 1970s. However, RCS is just one aspect of stealth, the design philosophy that seeks to make a platform (such as an aircraft, ship, or ground vehicle) undetectable to a wide range of sensors. Such a platform is referred to as low-observable (*LO*). In addition to radar, the infrared, acoustic, and visible signatures must be controlled. In the past, the RCS has received the most attention because the detection range of radar is generally much greater than that of other sensors. Undetectability does not necessarily imply a very low signature, only that the target must be indiscernible against the background. In the visible region (wavelengths visible to the eye) stealth has been used since World War II in the form of camouflage.

A typical radar and target arrangement is shown in Fig. 1. The transmitter illuminates the target from a distance R_t. If the body is sufficiently far from the transmitting antenna, the incident spherical wave front will be approximately planar across the target. The incident wave induces currents on the surface of the body, and even within its volume if the material is not a perfect electric conductor. The induced currents give rise to a scattered field, which is detected by the receiver at a distance R_r.

The arrangement shown in Fig. 1 is referred to as *bistatic;* the directions of the transmitter and receiver are different as viewed from the target. The *monostatic* case is more common; that is, the directions of the transmitter and receiver are the same as viewed from the target. For a truly monostatic radar the transmit and receive channels should use the same antenna. Frequently the radar will use separate antennas for transmit and receive, but they will be closely spaced on the same platform. This configuration is referred to as *quasimonostatic,* and can be considered as monostatic for the purpose of specifying the RCS of a distant target. The majority of radars currently in use for both military and civilian applications are monostatic.

Most radars are designed to provide information on the target's location and velocity. Location is given in terms of the range (radial distance) from the radar along with direction. The range to the target is obtained by a time delay measurement. An electromagnetic wave is transmitted in the direction of the target, and the round trip travel time converted to distance using the known velocity of propagation of the wave. The direction of the wave is obtained from antenna pointing. Velocity can be measured using the frequency shift due to the Doppler effect or two range measurements at closely spaced times to obtain the target's range rate. Any measurement of the target parameters assumes that the reflected wave is strong enough to be detected and processed by the radar. Search radars are specifically designed for this purpose. They are used to scan large volumes of space for targets at great distances (hundreds or even thousands of kilometers). Once a target has been detected it is handed over to a tracking radar. Modern multifunction radars are designed to perform both search and track functions.

Although both the search and track operations are more difficult for targets with low RCS, the primary objective of RCS reduction is to defeat search radars (i.e., avoid detection). The role of the RCS in the detection of a target is demonstrated by the basic form of the radar equation derived later. It shows that when all other

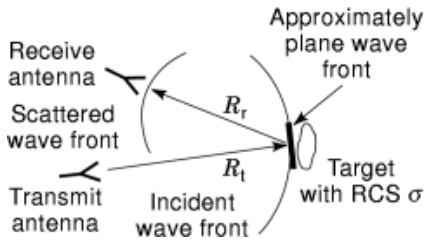

Fig. 1. Bistatic RCS refers to an arrangement where the transmitting and receiving antennas are at different locations as viewed from the target. For the monostatic case the transmitting and receiving antennas are co-located.

Table 1. Frequency Band Designations

Band Designation	Frequency Range
HF	3–30 MHz
VHF	30–300 MHz
UHF	300–1000 MHz
L	1–2 GHz
S	2–4 GHz
C	4–8 GHz
X	8–12 GHz
Ku	12–18 GHz
K	18–27 GHz
Ka	27–40 GHz
MM	40–300 GHz

radar system parameters are fixed, the maximum detection range of a target varies as the fourth root of RCS. Thus by reducing the target RCS, the range at which it is first seen by the radar is also reduced.

The RCS of modern aircraft and ships has been significantly reduced, but in response to the lower cross sections, more sensitive radars have evolved. The RCS designer is at a disadvantage in this respect because a truly LO platform must be designed from the start. Stealth cannot simply be added on after all other design tradeoffs have been made. The entire design and test cycle of an aircraft can be a decade, and its operational life several decades. On the other hand, the radar designer may be able to significantly increase the capability of a radar by simply replacing a system component such as an antenna or signal processor. These are relatively minor changes and can be integrated into deployed radars in a couple of years, thereby decreasing the effectiveness of the LO platform for the rest of its operational lifetime.

The scattering properties of the target are only one of several considerations that enter into the selection of the operating frequency of a radar (1,2). Others are size constraints, antenna gain and beam width, transmitter power, ambient noise, Doppler shift, and atmospheric attenuation. The frequency spectrum is divided into bands with letter designations as shown in Table 1. A few long-range ballistic missile defense radars operate in the 300 MHz region (UHF), but most others use frequencies greater than 1 GHz (L band and above). Devices at low frequencies are larger than similar devices at a higher frequency, and therefore the system's components require more volume. Likewise the antenna must be larger at a low frequency than at a high frequency to achieve the same beam width and gain. Low frequencies are capable of handling more power because the applied voltages can be higher without causing breakdown. Finally, ambient noise is lowest in the 1 to 10 GHz range, and low-altitude atmospheric attenuation favors frequencies below 18 GHz.

The function of the radar also influences the choice of frequency. For instance, an airborne imaging radar must be compact and lightweight, but also have a narrow antenna beam for resolving scatters. These all favor a high frequency. On the other hand, a ground-based search radar must radiate high power to achieve a large detection range. In this case the larger and heavier equipment that is necessary for high-power operation is not a problem.

Definition of Radar Cross Section

Radar cross section is defined as (3)

$$\frac{\text{power reflected towards receiver per unit solid angle}}{\text{incident power density}/4\pi}$$

In general it is dependent on many parameters. They include

(1) The size, shape, and material composition of the body
(2) The frequency and polarization of the incident electromagnetic wave
(3) The direction from which the wave illuminates the body, as well as that at which the observer is located (the angle at which the target is viewed is referred to as the *aspect angle*)

These factors are taken into consideration when a radar is designed to detect a specific target. On the other hand, if a vehicle is to face a radar with known specifications, the target can be designed with the radar's performance in mind. For example, if an aircraft will be flying directly at a radar in most mission scenarios, then it will be wise to put extra effort into reducing the nose-on RCS, perhaps even at the expense of raising it at broadside aspect angles. Furthermore, if the frequency of the radar is known, then the RCS reduction effort need only concentrate on that frequency.

The conventional symbol for RCS is σ and it has units of square meters. As evident in Table 2, typical values of the RCS range from 0.0005 m^2 for insects to 100,000 m^2 for a large ship. The decibel unit is convenient when working with quantities that extend over several orders of magnitude. The RCS in decibels relative to a square meter (dBsm) is defined as

$$\sigma_{\text{dBsm}} = 10 \log_{10} \sigma$$

Implicit in the definition of RCS is the assumption that the frequency is fixed.

Mathematically the RCS is given by

$$\sigma(\theta, \phi, \theta_i, \phi_i) = \lim_{R_r \to \infty} 4\pi R_r^2 \frac{|\boldsymbol{E}_s(\theta, \phi)|^2}{|\boldsymbol{E}_i(\theta_i, \phi_i)|^2} \qquad (1)$$

where

$\boldsymbol{E}_i$ = plane wave electric field intensity incident from the direction (θ_i, ϕ_i)
$\boldsymbol{E}_s$ = scattered spherical wave electric field intensity observed from the direction (θ, ϕ)
R_r = distance from the target to the observer as shown in Fig. 1

Table 2. Typical Values of RCS

Target	RCS (m^2)
Insects	0.0005
Small birds	0.01
People	0.5
Cars (front)	5–10
Fighter aircraft nose on broadside	10–50
Bomber aircraft	500–1000
Ships	1000–100000

At first glance is may appear that RCS is a function of range because of the R^2_r in Eq. (1). However, the scattered field is a spherical wave whose electric field has a $1/R_r$ dependence, which, when squared, cancels the factor in the denominator. Hence RCS is a range-independent quantity.

Electromagnetic scattering and radiation problems can be formulated in either the time domain (*TD*) or the frequency domain (*FD*) (4,5). In fact, the scattering body can be represented as a linear system with impulse and frequency responses. The RCS as a function of time is related to the RCS as a function of frequency by the Fourier transformation. There are advantages and disadvantages to working in each domain. Early radar systems operated over narrow frequency ranges, and the need to compare calculated and measured data dictated that calculations also be done in the frequency domain. Modern radars operate over wide frequency ranges, and in order to characterize their performance adequately, the target RCS must also be determined over the same wide range of frequencies. For a large, complex target, the calculation of the RCS at each frequency is potentially a time-consuming task. It may be more efficient to compute the target's response to a waveform in the time domain and then perform a Fourier transformation to obtain the RCS at many frequencies simultaneously. Thus the measurement or calculation of RCS can be performed by either of two procedures:

(1) Frequency Domain The received power is obtained as the target is rotated through a range of angles while a continuous wave (*CW*) fixed-frequency source is radiating. The frequency can be changed and another plot of RCS versus angle obtained, and so on. At any fixed angle the RCS from a large number of frequencies can be Fourier transformed to obtain the time-domain response of the target at that particular angle.
(2) Time Domain The received power as a function of time is obtained at each aspect angle of interest. The time histories are inverse Fourier transformed to yield the frequency response of the target at each angle. If the Fourier transform of the waveform and the impulse response of the radar system are known, then the target's frequency response can be converted to RCS.

There are several aspects of the RCS that enter into the design of an LO platform, and therefore the discussion of the RCS logically falls along similar lines. They include the topics:

(1) Electromagnetic (*EM*) scattering mechanisms and the physical aspects of scattering
(2) Analytical and computational methods
(3) Reduction methods
(4) Measurement techniques

A brief overview of each of these four topics is given, followed by mathematically based discussions of RCS prediction and reduction.

Basic Scattering Characteristics of Bodies

Frequency Regions. The scattering characteristics of a target are strongly dependent on the frequency of the incident wave. There are three frequency regions in which the RCS of a target is distinctly different. They are referred to as the (1) low, (2) resonance, and (3) high frequency regimes (6). The labels are somewhat misleading in that low and high are defined relative to the size of the target when normalized to the incident wavelength, rather than to its physical size. If the target is smooth and it can be roughly described by a characteristic length L, then the three frequency regimes can be defined in terms of the quantity βL, where

$$\beta = 2\pi/\lambda \qquad (2)$$

and λ is the wavelength.

Low Frequency Region ($\beta L \ll 1$) At these frequencies the phase variation of the incident plane wave across the extent of the target is small. Thus the induced current on the body is approximately constant in amplitude and phase. The particular shape of the body is not a factor in the RCS pattern shape. For example, both a small sphere and a small cube have essentially isotropic (direction-independent) scattering patterns. In general, σ versus βL is smooth and varies as λ^{-4}. This region is also called the Rayleigh region.

Resonance Region ($\beta L \approx 1$) When βL is on the order of 1, the phase variation of the incident field across the body is significant and all parts contribute to the scattering pattern. A plot of σ versus βL is oscillatory. This region is also referred to as the Mie region.

High Frequency Region ($\beta L \gg 1$) There are many cycles in the phase variation of the current across the body, and consequently the scattered field will be very angle-dependent. The peak scattering levels are primarily due to isolated points. For example, the peak scattering from large flat plates originates from specular points on the surface. (They are the mirrorlike reflection points for which the angle of reflection equals the angle of incidence.) A plot of σ versus βL is smooth in this region and may be independent of λ. This is also called the optical region.

The RCS of a sphere, which is plotted in Fig. 2, clearly illustrates the three frequency regions. The appropriate characteristic dimension of the sphere is its radius; therefore, let $L = a$. (One could argue that based on the previous discussion that $L = 2a$ should be used. However, the boundaries between the frequency regions are defined by orders of magnitude; they are not sharp. Hence either choice for L is acceptable. For a sphere quantities are generally normalized to the radius, and therefore $L = a$ is the most convenient choice.) For $\beta a < 1$, the curve is almost linear, but above 1 it begins to oscillate. This is the resonance region. The oscillations die out at higher values, and above $\beta a \leq 10$ the curve approaches a constant equal to πa^2.

Polarization and the Scattering Matrix. In addition to frequency, polarization plays a major factor in determining the scattering characteristics of a body. Polarization refers to the orientation of the electric field vector. The incident wave polarization is determined by the orientation of the transmit antenna, while the receive antenna determines the receive polarization. If the antennas are linearly polarized and their electric field vectors are aligned, then the copolarized scattered field is measured. On the other hand, if linear transmit and receive antennas are orthogonal (electric field vectors crossed at 90°), then the cross-polarized component of the scattered field is sensed.

The copolarized scattered field is generally used, for several reasons. First, the copolarized scattered field component is usually much higher than the cross-polarized component. Secondly, for monostatic radars it is more efficient to use the same antenna for transmit and receive, and hence the transmit and receive

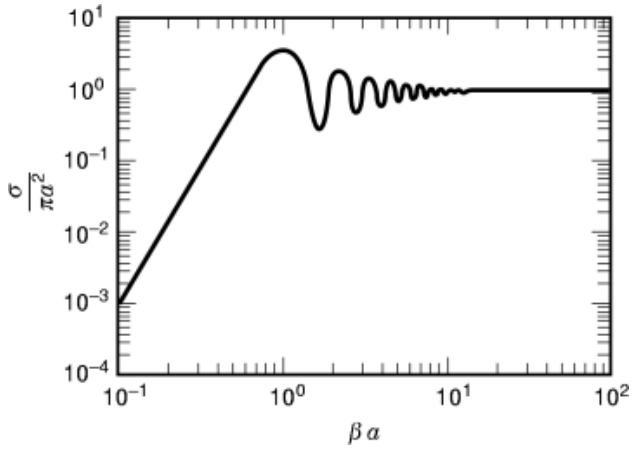

Fig. 2. The RCS of a sphere illustrates the three frequency regions: (1) Rayleigh (linear region at low frequencies), (2) resonance (oscillatory region), and (3) optical (flat high frequency region).

polarizations are identical. However, measuring both components provides the most information available from the scattered field and may assist in target identification.

A polarization-specific RCS can be expressed as

$$\sigma_{qp} = \lim_{R_r \to \infty} 4\pi R_r^2 \frac{|\boldsymbol{E}_{sq}|^2}{|\boldsymbol{E}_{ip}|^2} \tag{3}$$

where p denotes the polarization of the incident wave and q the polarization of the receiver. Common polarization designations are defined with regard to a reference such as the ground or surface. They include: horizontal and vertical (H and V); parallel and perpendicular ($\parallel$ and $\perp$); rectangular (x and y). A scattering matrix relates the scattered field components to the incident field components:

$$\begin{bmatrix} E_{s\theta} \\ E_{s\phi} \end{bmatrix} = \begin{bmatrix} S_{\theta\theta} & S_{\theta\phi} \\ S_{\phi\theta} & S_{\phi\phi} \end{bmatrix} \begin{bmatrix} E_{i\theta} \\ E_{i\phi} \end{bmatrix} \tag{4}$$

The elements of the scattering matrix can be determined by computation or measurement.

The RCS of a cylinder illustrates the effect of polarization on scattering level and pattern shape. As shown in Fig. 3, a relatively strong copolarized RCS exists even for thin wires, whereas the cross-polarized RCS tends to zero. At high frequencies the cross sections for both polarizations asymptotically approach the same value.

Monstatic versus Bistatic RCS. The vast majority of radars currently in use are monostatic, because most systems must operate from a single platform. However, the monostatic RCS (backscatter) of electrically large smooth flat targets is very small unless the radar is positioned normal to the surface. Besides the normal, large cross sections are observed in the specular ($\theta = \theta_i$) and forward ($\theta = \theta_i + \pi$) scattering directions.

Bistatic radars have the transmit and receive antennas in two separate locations. Thus a bistatic radar with a receiver at either of these two locations would have the advantage of larger target RCS. However there are also disadvantages such as reduced operational flexibility because of the restricted transmit–receive relationships, and maintaining a coherent reference for the transmitter and receiver.

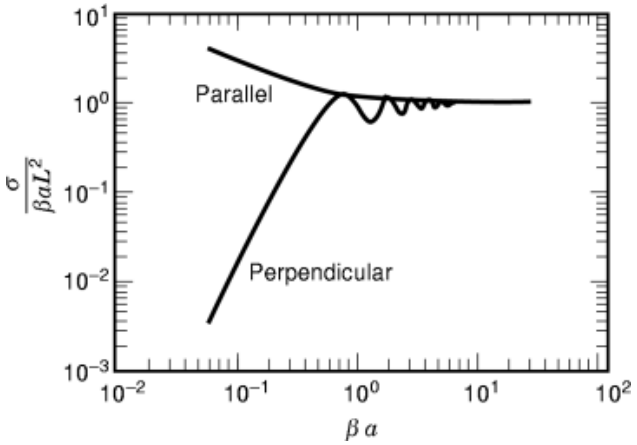

Fig. 3. A cylinder illustrates how a target's RCS can depend on the incident wave polarization. At low frequencies the cylinder becomes a thin wire that is transparent to a perpendicularly polarized wave.

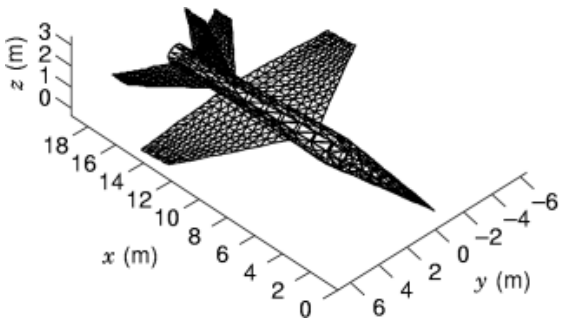

Fig. 4. Simple geometric shapes such as plates, cylinders, and spheres can be used to build more complicated targets. The interaction between the individual parts is important in determining low-level RCS.

Scattering Mechanisms

The RCSs of targets encountered by most radars are complicated geometrical shapes. There are a few exceptions such as weather balloons and buoys. However, simple shapes such as plates, spheres, cylinders and wires are useful in studying the phenomenology of RCSs. Furthermore, complex shapes can be decomposed into basic geometrical building blocks (primitives) that can be assembled to form a more complex shape. Figure 4 shows an aircraft represented by cylinders, plates, cones, and hemispheres. The RCS of the model in Fig. 4 is shown in Fig. 5. A collection of basic shapes gives an acceptable RCS estimate that can be used during the initial design stages of a platform. The locations and levels of the largest RCS lobes are of most concern at this stage of the design process. The accuracy of the RCS estimate at other angles depends on how the interactions between the various shapes are handled. These are more difficult to include, as will be seen later. Even when they are included, the agreement with the measured RCS may not be particularly good if the interactions are not modeled accurately. For an LO target more sophisticated numerical techniques must be used.

As evident from the pattern in Fig. 5, the RCS of a large, complex target is a rapidly varying function of angle. However, as complicated as it looks, isolated features of the pattern shape and level can be associated with the behavior of the currents induced in and on the scattering body. For example, the high narrow spikes

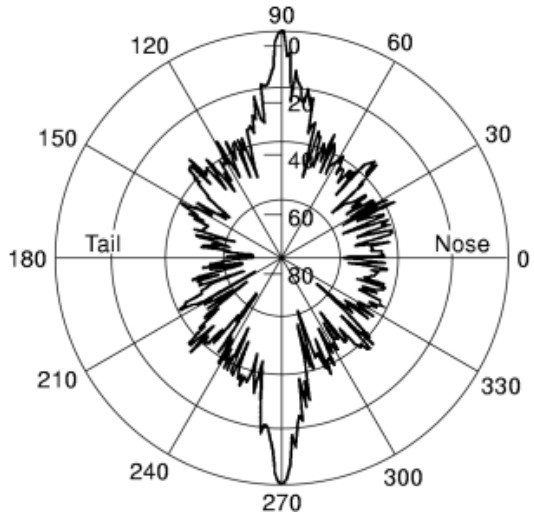

Fig. 5. An azimuth plot of the RCS of the aircraft in Figure 4 is shown. The two large lobes are due to the fuselage, which is modeled as a cylinder.

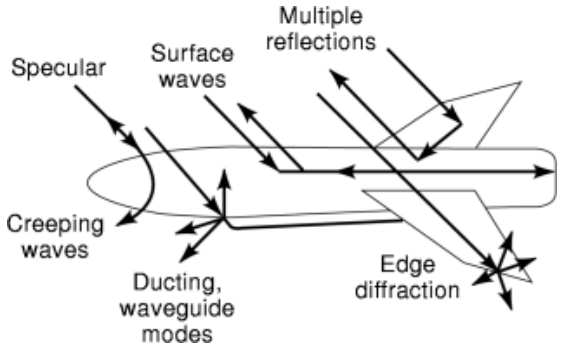

Fig. 6. The total RCS of a target can often be decomposed into a sum of contributions from distinct scattering mechanisms. Some important mechanisms for electrically large targets are depicted in this figure.

result from mirrorlike specular reflections from large flat surfaces. Other lobes can be associated with surface waves, multiple reflections, diffraction, and so on. These so-called scattering mechanisms are depicted in Fig. 6. The lines in the figure are ray representations for propagating waves. They denote the direction of power flow and are normal to the planes of constant phase.

For any particular aspect angle, frequency, and polarization, if one scattering mechanism dominates over all others, then it may be possible to express the total scattered field as a combination of scattered fields $\boldsymbol{E}_{s1}$, $\boldsymbol{E}_{s2}$, $\boldsymbol{E}_{s3}$, ..., each due to a separate scattering mechanism:

$$\boldsymbol{E}_s \approx \boldsymbol{E}_{s1} + \boldsymbol{E}_{s2} + \boldsymbol{E}_{s3} + \cdots$$

and if one of these terms is much greater than all others,

$$|\boldsymbol{E}_s|^2 \approx |\boldsymbol{E}_{s1}|^2 + |\boldsymbol{E}_{s2}|^2 + |\boldsymbol{E}_{s3}|^2 + \cdots$$

It follows from Eq. (1) that the total RCS can be written as a sum of RCSs, each attributed to a separate scattering mechanism:

$$\sigma \approx \sigma_{s1} + \sigma_{s2} + \sigma_{s3} + \cdots \tag{5}$$

Note that Eq. (5) is a convenient way of decomposing the scattered field for the purpose of assisting the RCS modeling and reduction efforts. First, if sufficiently accurate models exist for the individual scattering mechanisms, then Eq. (3) suggests that they can be combined under the appropriate circumstances to model their collective effects for a complex target. Secondly, since the largest terms in Eq. (3) correspond to the source of the most intense scattering, it may be possible to determine which scattering mechanism dominates, and thereby choose an appropriate reduction technique.

Reflection. This is the mechanism that yields the highest RCS peaks, but they are limited in number because Snell's law must be satisfied. When multiple surfaces are present, multiple reflections are possible. For instance, the incident plane wave could reflect off of the fuselage of an aircraft, hit a fin, and then return to the radar.

Diffraction. Diffracted fields are those scattered from discontinuities such as edges, corners, and vertices. The waves that are diffracted from these shapes are less intense than reflected waves, but they can emerge over a wide range of angles. At aspects requiring low RCS, the diffracted waves can be significant.

Surface Waves. The term *surface wave* refers to the current traveling along a body and includes several types of waves (7). In general, the target acts as a transmission line, guiding the wave along its surface. If the surface is a smooth closed shape such as a sphere, the wave can circulate around the body many times. Such waves are called creeping waves because they appear to creep around the back of a curved body. On curved bodies the surface wave continuously radiates. Radiating surface waves on flat bodies are usually called *leaky waves. Traveling waves* appear on slender bodies and along edges, and suffer little attenuation as they propagate (8). If the surface is terminated with a discontinuity such as an edge, the traveling wave will be reflected back along the surface and radiate towards its origin.

Ducting. Also called waveguide modes, ducting occurs when a wave is trapped in a partially closed structure. An example is an air inlet cavity on a jet. Once the wave enters the cavity, many bounces can occur before a ray emerges. There are many paths that the ray can take, and therefore rays emerge at almost all angles. The result is a large, broad monostatic RCS lobe. An optical analogy of this is the glowing of a cat's eye when it is illuminated by a light.

Interactions. It is possible that these mechanisms will interact with each other. For example, a wave reflected from a flat surface can subsequently be diffracted from an edge or enter a cavity. For a complex target the interactions are not always obvious and the decomposition of the scattered field no longer makes sense.

Prediction Methods

The analytical methods used to calculate RCSs are similar to those used in antenna analysis. A radar target is essentially acting as an antenna. The incident wave induces a current on the target, and the induced current radiates a field just as an antenna would. However, in the radar case it is called a scattered field as opposed to a radiated field. A good example is a reflector antenna or "satellite dish." The incident field from a feed horn excites currents on the reflector, which in turn give rise to a radiated field. In the radar analogy, the feed horn represents the radar's transmit antenna, while the reflector is the target. If the distribution of current is known for a target, then the currents can be used in the radiation integrals (Stratton–Chu integrals) to determine the scattered field. Once the scattered field is known, the RCS can be computed.

Of course, the problem is that the induced current on the target is unknown and generally very difficult to determine. An analytical solution is possible in only a few simple cases. In other cases it is feasible to solve Maxwell's equations or integral equations for the current numerically. These solutions are rigorous in that there are no assumptions or restrictions imposed. The only error in the solution is due to the numerical evaluation of the integral or differential equations. The alternative to a numerical solution is to take an intuitive guess at the current, in which case the resulting RCS is only approximate.

Several methods of RCS prediction are described below. The classical solution techniques are not discussed in this list, because most are limited to one- or two-dimensional structures or simple three dimensional ones. The methods of interest here are those that can be applied to complex three-dimensional targets. The methods most commonly encountered are physical optics, microwave optics (ray tracing), the method of moments, and finite-difference methods.

Physical Optics. The physical optics (*PO*) approximation (9) provides a means of estimating the surface current induced on an arbitrary body. On the portions of the body that are directly illuminated by the incident field, the induced current is simply proportional to the incident magnetic field intensity. On the shadowed portion of the target the current is assumed to be zero. The current is then used in the radiation integrals to compute the scattered field far from the target.

PO is a high-frequency approximation that gives best results for electrically large bodies ($L \geq 10\lambda$). It is most accurate in the specular direction. Since PO assumes that the current abruptly decays to zero at a shadow boundary, the computed field values at angles far from the specular directions and in the shadow regions are inaccurate. Furthermore, surface waves are not included. PO can be used in either the time or the frequency domain. It can be supplemented by the physical theory of diffraction (*PTD*), which provides corrections to PO approximation that improve the accuracy of the current distribution near edges.

Microwave Optics. Microwave optics refers to a collection of ray-tracing methods that can be used to analyze electrically large targets of arbitrary shape. The rules for ray tracing in a simple medium (linear, homogeneous, and isotropic) are similar to reflection and refraction in optics. Geometrical optics (*GO*) (10) is the classical theory of ray tracing used since the days of Newton. It provides a formula for computing the reflected and refracted fields. In addition, the geometrical theory of diffraction (*GTD*) is used in conjunction with GO to include diffraction. Diffracted rays originate from the scattering of the incident wave at edges, corners, and vertices. The formulas are derived on the basis of infinite frequency ($\lambda \to \infty$), which implies an electrically large target. Ray optics is frequently used in situations that severely violate this restriction and still yields surprisingly good results. The major disadvantage of ray tracing is the bookkeeping required for a complex target. It is used primarily in the frequency domain.

Method of Moments. The method of moments (*MM*) is a technique used to solve an integral equation (11). Integral equations are so named because the unknown quantity appears in an integrand. In electromagnetics they are derived from Maxwell's equations and the boundary conditions. The unknown quantity can be a combination of volume or surface current (either electric or magnetic). The MM reduces the integral equations to a set of simultaneous linear equations that can be solved using standard matrix algebra. The size of the matrix involved depends on the size of the body; current computer capabilities allow bodies on the order of 10 or 20 wavelengths to be modeled.

Most MM formulations require a discretization (segmentation) of the body. Therefore, they are compatible with finite-element methods used in structural engineering, and the two are frequently used in tandem during the design of a platform. The MM can be used to solve both time- and frequency-domain integral equations.

Finite-Difference Methods. Finite differences are used to approximate the differential operators in Maxwell's equations in either the time or the frequency domain (5,6). As with the MM technique, the target and surrounding space must be discretized. Maxwell's equations and the boundary conditions are enforced on the surface of the target and at the boundaries of the discretization cells. This method has found extensive use in computing the transient response of targets to various waveforms. Finite-difference methods do not require the large matrices that the MM does, because the solution is stepped in time throughout the scattering body.

Reduction of Radar Cross Sections

RCS reduction techniques are traditionally classified as geometrical shaping, materials selection, and passive and active cancellation. The boundaries between these categories are not always distinct, and a reduction approach may draw on all of these simultaneously.

Shaping. Target shaping is the first step in RCS reduction. The first rule of shaping is to avoid presenting large flat surfaces to the radar. For large surfaces specular reflection is the dominant scattering mechanism. The direction of strongest reflection for a smooth surface is given by the law of reflection. Therefore, by examining the relationship between the direction of incidence and the surface normal, the direction of maximum scattering can be predicted. If a target is composed of several surfaces and one could visualize a plot of the normals of the surfaces, then it is expected that there would be few normals pointed in directions of low RCS.

It will be shown that the maximum monostatic RCS of a large flat surface occurs when the incident wave and observer are located normal to the surface. The maximum value is

$$\sigma_{\mathrm{m}} = \frac{4\pi A^2}{\lambda^2} \tag{6}$$

where A is the area of the surface. Thus the RCS can be minimized by minimizing the area presented to the radar. If it is not possible to tilt a large surface sufficiently, then it can be broken into a number of smaller surfaces, each tilted in a slightly different direction.

These approaches have led to rather unconventional aircraft shapes such as that of the F-117 Nighthawk (commonly referred to as the "Stealth Fighter") (12). To date, shaping has not been applied extensively to ships and ground vehicles, although that is beginning to be done. Modern ship designs are making some concessions to RCS control, such as canting deckhouse walls and enclosing mast structures.

Another aspect of shaping is edge alignment. Once the specular reflections have been controlled, the contributions from edges (such as traveling waves and diffraction) may become important. Aligning edges is one way of maintaining low-RCS spatial sectors. For example, in plan form it is seen that the edges of the B2 bomber fall along only a couple of fixed angles.

The second rule of shaping is to avoid or hide retroreflectors. Retroreflectors are simple geometrical structures that tend to redirect the incident radar wave back in the direction from which it arrives. Surfaces that meet at a 90° angle are strong retroreflectors, and therefore the angles between the tail rudder and elevator surfaces of a stealthy aircraft are always canted. New designs such as the tailless McDonnell Douglas X-36 have no vertical surfaces at all.

Cavities are another type of retroreflector. They have a very broad scattering pattern. Thus jet intakes are often located above the wing or else employ an electromagnetic screen to prevent penetration by the incident wave.

Obviously there is a limit to the degree of shaping that can be incorporated while simultaneously meeting other operational requirements. For example, extreme shaping applied to an aircraft degrades its aerodynamic performance and control characteristics. Another disadvantage of low-RCS shapes is that they have slim profiles, which reduces the useful enclosed volume relative to a conventional shape.

Materials and Coatings. Obviously the material composition of a body affects its RCS. For example, a metal plate has a higher RCS than a glass plate. Similarly, a plastic aircraft body has a lower RCS than one with a metal skin. The electrical characteristics of a material are defined by its constitutive parameters (13):

(1) Permittivity, $\varepsilon = \varepsilon_0\varepsilon_{\mathrm{r}} = \varepsilon' - j\varepsilon''$ (F/m)

(2) Permeability, $\mu = \mu_0\mu_{\mathrm{r}} = \mu' - j\mu''$ (H/m)

(3) Conductivity, σ_{c} (Ω/m)

where ε_0 and μ_0 are the permittivity and permeability of free space. The imaginary parts are associated with dissipation (attenuation) of the fields in the medium.

The permittivity determines the fundamental relationship between the electric field intensity $\boldsymbol{E}$ and flux density $\boldsymbol{D}$. For the vast majority of materials that occur in nature one can write

$$\boldsymbol{D} = \boldsymbol{\epsilon}\boldsymbol{E} \tag{7}$$

where the boldface ε denotes a matrix. Expanding Eq. (7) and explicitly including the spatial and frequency dependences gives

$$\begin{bmatrix} D_x \\ D_y \\ D_z \end{bmatrix} = \begin{bmatrix} \epsilon_{xx}(x,y,z,f) & \epsilon_{xy}(x,y,z,f) & \epsilon_{xz}(x,y,z,f) \\ \epsilon_{yx}(x,y,z,f) & \epsilon_{yy}(x,y,z,f) & \epsilon_{yz}(x,y,z,f) \\ \epsilon_{zx}(x,y,z,f) & \epsilon_{zy}(x,y,z,f) & \epsilon_{zz}(x,y,z,f) \end{bmatrix} \begin{bmatrix} E_x \\ E_y \\ E_z \end{bmatrix} \tag{8}$$

Likewise, the permeability determines the fundamental relationship between the magnetic field intensity $\boldsymbol{H}$ and magnetic flux density $\boldsymbol{B}$, which for most materials can be written as

$$\boldsymbol{B} = \boldsymbol{\mu}\boldsymbol{H}$$

or

$$\begin{bmatrix} B_x \\ B_y \\ B_z \end{bmatrix} = \begin{bmatrix} \mu_{xx}(x,y,z,f) & \mu_{xy}(x,y,z,f) & \mu_{xz}(x,y,z,f) \\ \mu_{yx}(x,y,z,f) & \mu_{yy}(x,y,z,f) & \mu_{yz}(x,y,z,f) \\ \mu_{zx}(x,y,z,f) & \mu_{zy}(x,y,z,f) & \mu_{zz}(x,y,z,f) \end{bmatrix} \begin{bmatrix} H_x \\ H_y \\ H_z \end{bmatrix} \tag{9}$$

The following special cases occur frequently:

(1) Isotropic
(2) The diagonal components of the permittivity and permeability matrices are equal, and the off-diagonal elements are zero. That is, $\varepsilon_{pp} = \varepsilon_r\varepsilon_0$ and $\mu_{pp} = \mu_r\mu_0$; $\varepsilon_{pq} = 0$ and $\mu_{pq} = 0$ if $p \neq q$ ($p, q = x, y,$ or z).
(3) Nondispersive
(4) The constitutive parameters are independent of frequency. Most materials exhibit some dispersion (frequency dependence) if the frequency change is great enough. However, we define a nondispersive material as one whose ε_r and μ_r are sufficiently constant within the frequency band of the radar illuminating the material.
(5) Homogeneous
(6) The constitutive parameters are independent of location in the material. Almost all materials are inhomogeneous on a microscopic scale. For our purpose a homogeneous material is one that has a sufficiently small variation in ε_r and μ_r throughout its volume.

To examine the dependence of the RCS on the constitutive parameters, consider an infinite interface between free space and a half-space of material with ε_r and μ_r. The Fresnel reflection coefficient for a plane

wave normally incident on the interface is

$$\Gamma = \frac{\eta_l - \eta_0}{\eta_l + \eta_0} \tag{10}$$

where the intrinsic impedances are defined by

$$\eta_0 = \sqrt{\frac{\mu_0}{\epsilon_0}}$$

and

$$\eta_l = \sqrt{\frac{\mu_r \mu_0}{\epsilon_r \epsilon_0}} = \eta_0 \sqrt{\frac{\mu_r}{\epsilon_r}}$$

From Eq. 1 the RCS is proportional to the square of the scattered electric field intensity. Since the scattered field intensity (in this case the reflected field) is proportional to Γ, it follows that $\sigma \propto |\Gamma|^2$. Thus the RCS will be reduced in direct proportion to the reduction in reflection coefficient squared. This is an ideal limit, because in practice the material thickness is finite, and there will likely be some reflection from its back face and scattering from its edges.

Unfortunately, in most applications the target materials cannot be selected solely on the basis of the electromagnetic properties ε_r and μ_r. Mechanical properties such as strength, weight, and thermal conductivity have a higher priority. In the drive to reduce weight and increase strength, composite materials have found widespread military and civilian application (14).

Composites are formed from multiple constitutive materials in a manner that yields a final product having desirable properties from each material. Graphite is an example of a composite that is used extensively in the aircraft industry. Although the primary motivation for the use of composites has been structural, the reflection from most composite materials is lower than that for conductors. However, the majority of the incident field that is not reflected from the composite's surface is transmitted through the material, and the transmitted field can potentially be scattered from internal metallic objects. The use of nonconductors also complicates other electrical design issues such as the grounding of electrical systems and lightning protection.

An absorbing layer is another example of the application of materials for RCS reduction. A layer of absorbing material is deposited on the surface of the target. As the incident wave propagates through the material, energy is extracted from the field and its intensity diminishes (15). Thus a weaker field is reflected at the target surface, and the reflected wave is attenuated further as it travels back through the material. The circuit analog of this type of material is a resistor.

A material that performs the function just described is referred to as a radar absorbing material (*RAM*). High absorption is desired, yet the material thickness and weight must be minimized. Unfortunately, many materials with high loss also have high reflection coefficients. Thus there is significant reflection of the incident wave at the absorbing-layer face, and little energy enters the material where attenuation takes place.

There are some materials that possess more complicated or exotic electromagnetic properties that can potentially be exploited for RCS reduction. For example, since the ε_{pq} affect the velocity of propagation along the coordinate axes of the material, it may be possible to construct ε for a material so that the polarization of the scattered field is different than that of the incident field. Thus the polarization of a wave rotates as it propagates through the medium, and scattered energy is converted to a field component that the radar is not capable of sensing.

Another example is a spatially dispersive medium. The electric flux density depends on both the electric field intensity and the magnetic flux density. A *chiral* material (16) has the constitutive relationship

$$\boldsymbol{D} = \epsilon \boldsymbol{E} + j\xi \boldsymbol{B}$$

This type of behavior is associated with materials that have a helical molecular structure. It is possible to produce this type of behavior artificially by dispersing small helical coils throughout a bulk material.

In the past, the reduction of RCSs has focused on treating each scattering source, or hot spot, individually. For instance, an absorbing layer might be installed to reduce scattering from a wing edge. The layer will reduce the edge scattering, but will also introduce new scattering sources at the perimeter. For a useful reduction method, the new scattering sources must be much weaker than those of the original edge. But as the scattering intensities of the sources become smaller, one quickly reaches the point where the new scattering sources introduced by the treatments are comparable to those being treated. At this level the interaction between scatterers becomes important, and this complicates the design and application of RCS treatments.

Cancellation Techniques. Cancellation refers to RCS reduction methods that are based on the introduction of a secondary scatterer whose scattered field is adjusted to cancel the reflection of the primary target (17,18). The total field at the radar receiver is the vector sum of the fields scattered by the target and the cancellation element. Therefore, if the cancellation field can be made equal and opposite to the field scattered from the body at the angle, polarization, and frequency of interest, then destructive interference occurs. The secondary scatterer is referred to as the *cancellation element,* and its scattered field the *cancellation field.*

The cancellation element can be a detached body located near the original target, or an attached protrusion. Both are referred to as *parasitic* elements. The combination of the target with the scattering element is frequently called the *loaded body.* If the cancellation field is fixed, then the system is a *passive* one. On the other hand, if the system can respond to changes in the incident field, then it is an *active* one. A fair amount of information about the radar and the target is required for an active system: the threat radar frequency, its direction and polarization, and the target's RCS in the direction of the radar.

Passive Cancellation. Since the cancellation of the two fields is essentially a tuning method, this technique is only effective over a narrow frequency band and usually limited to a small spatial sector. If large parasitic elements are to be avoided, then the magnitude of RCS that can be canceled is small. Thus passive cancellation is usually used to supplement shaping and absorbers.

The most common cancellation elements are slots and wires. Two orthogonal elements are required to cancel an incident wave of arbitrary polarization. The elements can be increased in size or number so as to provide sufficient gain to cancel the RCS in the direction of interest.

Two examples of passive cancellation are the Salisbury screen and Dallenbach layer (19). A Salisbury screen consists of a resistive film located a distance d in front of the target surface. The film resistivity is chosen so that the reflection from its surface is exactly canceled by the field that passes through the film, is reflected from the target, and then is transmitted back through the film.

The Dallenbach layer shown in Fig. 7 is similar to the RAM coating discussed earlier, except that the layer thickness is chosen to provide destructive interference between the fields scattered from the top of the layer and the boundary at the back of the layer, rather than absorption within it. Thus the top of the layer serves the same purpose as the resistive film does for the Salisbury screen.

Active Cancellation. Active cancellation (also known as adaptive cancellation) is the extension of passive cancellation to handle dynamic threat scenarios. In the context used here, it does not include *deception,* which comprises techniques of modifying and retransmitting a signal. For the present discussion, the source of RF energy is the radar's signal. Two levels of sophistication are considered:

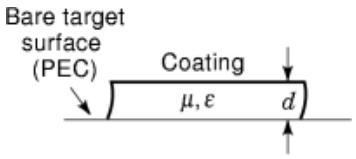

Fig. 7. A Dallenbach layer is used to reduce the RCS of a conductor. The material electrical characteristics and thickness are chosen to provide a reflection coefficient of zero.

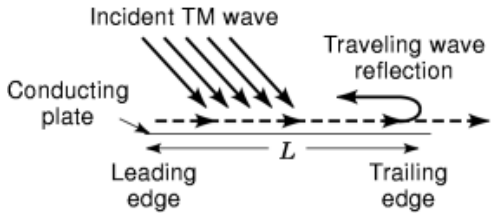

Fig. 8. Traveling waves along a surface are treated using a transmission line matching method: the quarter wave transformer.

(1) Fully active The cancellation network receives, amplifies, and retransmits the threat signal in such a way that it is out of phase with the static (skin) RCS of the target. The transmitted signal amplitude, phase, frequency, and polarization can be adjusted to compensate for changing threat parameters.

(2) Semiactive No amplification of the incident signal energy is provided by the cancellation network, but adjustable devices in the network allow the reradiated signal to compensate for limited changes in the radar signal parameters.

The demands for a fully active system are almost always so severe as to make it difficult to implement. It requires amplifiers and antennas that cover the anticipated threat angles, frequencies, incident power densities, and polarizations. A knowledge of the radar's direction is required, as well as the target's own RCS. A semiactive system is not as complicated with regard to hardware, but the use of adjustable devices still requires bias lines, controller units, and a computer with the appropriate databases.

Because of the growing importance of low-level scattering sources (in particular, manufacturing-induced errors that differ from platform to platform), adaptive cancellation techniques are receiving increased attention. Adaptive cancelers have the ability to modify the amplitude and phase of the new scattering source to compensate for changes in the original scattering source that may occur with frequency or observation angle. In principle, adaptive techniques are capable of adjusting to changing physical and electrical conditions brought on by exposure to the environment. However, cancellation is most effective when there are a small number of coherent scattering sources rather than a large number of random sources.

Treatments for Surface Waves. Surface waves, and in particular traveling waves, present a special challenge as far as RCS reduction is concerned (6). The target acts as a combination of antenna and transmission line, collecting incident energy and guiding it along the surface. As depicted in Fig. 8, when a discontinuity (such as a termination) is encountered, the surface wave is reflected. As it propagates in the reverse direction, it loses energy by radiation. A dielectric-coated ground plane can support a surface wave for incident plane waves having a component of $\boldsymbol{E}$ normal to the surface; a magnetic-coated ground plane can support a surface wave for incident plane waves having a component of $\boldsymbol{H}$ normal to the surface.

The most common technique for treating surface-wave reflections that arise from surface discontinuities is one borrowed from transmission line theory: the use of transformer sections. Typically a quarter-wave matching section is appended to the termination of the surface, and the surface characteristics of the matching

section are chosen to allow the wave to continue propagating in the forward direction, thereby eliminating the reflected field.

Special Stealth Issues

To achieve and maintain low observability requires careful design, manufacturing and maintenance procedures to a level that may seem trivial to the nonspecialist. Instances of bird droppings, loose screws, and pebbles kicked up from the takeoff roll having resulted in increased RCS have been reported (12). Some special stealth-related issues are discussed below.

Integration of Sensors and Sensor RCS. Active sensors that transmit energy, such as microwave and laser radars, need to have a low probability of intercept (*LPI*). One aspect of LPI involves controlling the spatial distribution of radiation by using narrow antenna beams and low sidelobes. Another is to control the power distribution in the frequency spectrum, which is directly related to the transmitted waveform. For example, wide-bandwidth spread-spectrum pseudorandom waveforms distribute their power almost uniformly over a wide frequency band and hence appear like noise, making detection extremely difficult.

The RCSs of sensors installed on an LO platform, especially antennas in the radar frequency bands, are an area of concern. Unlike cavities, antennas cannot always be hidden from the radar's field of view without degrading the performance of the accompanying system. Ideally, if the incident wave frequency is in the operating band of the antenna (where the antenna is efficient), then its RCS is low because most of the incident wave is collected and appears at the antenna terminals.

The antenna scattering occurs when the frequency of the radar wave is outside the antenna's operating band. Large reflection sources may occur inside the antenna at frequencies out of its operating band, resulting in scattering characteristics similar to those of a cavity. Furthermore, if the antenna is composed of widely spaced (relative to wavelength) periodic elements, Bragg diffraction can occur. Bragg lobes are high-RCS spikes that result at multiple angles when the round trip path length differences between adjacent elements are an integer multiple of 2π. (This is similar to array grating lobes in the radiation case.)

The obvious antenna RCS reduction methods, such as adding lossy materials to attenuate out-of-band reflections, also decrease the antenna's gain in its operating band. The preferred approach is to incorporate a frequency-selective surface (*FSS*) into the design. An ideal FSS permits radiation in the antenna's frequency band to pass through unattenuated while all other frequencies are reflected or absorbed. FSS shielding has been applied to antennas on ship masts (20) and as missile radomes (21).

In the drive to reduce the number of low-level scattering sources, continuity of the platform external surface should be maintained. The number of apertures (openings) must be kept to a minimum. Apertures are needed for radar and communication antennas, which operate at microwave frequencies, and infrared and optical sensors. By integrating the infrared and optical sensors into the antennas, two or three apertures can be replaced by a single one.

Computational Advances. The need to predict the mutual interactions between many low-level scattering sources has fueled research in the area of computational electromagnetics (*CEM*). Numerical solutions of the rigorous equations of scattering from complex bodies have existed since the early 1960s. They involve reducing the electromagnetic equations to a set of simultaneous linear equations, which are solved by matrix methods. The dimension of the matrix increases as the size of the target measured in wavelengths increases (that is, all target dimensions are scaled by the wavelength of the incident wave). It has only been in recent years that the dramatic increase in computer memory and speed has made this approach practicable for aircraft and ships. Even so, rigorous methods are still limited to low frequencies for targets that are physically large.

Approximate solutions have been developed based on the assumption that scattering is localized, so that interactions between distant parts of the structure can be neglected. The approximations have constantly been

improved by adding higher-order corrections based on ever more detailed electromagnetic models as well as empirical data. Both the rigorous and the approximate computer models have incorporated geometry builders that can utilize computer-aided drawing (*CAD*) files generated by commercially available drawing programs. This capability allows for *concurrent engineering*—the ability to make a structural change and immediately assess its effect on the RCS.

Effect of Imperfections and Flaws. An important limitation in achieving low RCS is the imperfections introduced during the manufacture and assembly of the platform and the installation of its systems. Their effect on RCS performance depends on whether the imperfections are periodic or random in nature. Most error sources are nearly random, and their net effect on RCSs is to shift energy from the scattering mechanisms discussed previously to diffuse scattering. Diffuse surfaces reflect uniformly in all directions, independent of the angle of incidence; they are electrically rough surfaces. The magnitude of the diffuse scattering increases with the extent of the surface roughness (imperfection). Since diffuse scattering is not angle-dependent, shaping is not a practical way of reducing the RCS for it, and therefore very close tolerances must be maintained to keep the diffuse scattering to acceptable levels. Maintaining close tolerances is one of the primary cost drivers in the manufacture of LO platforms. Eventually a point is reached where the question must be asked: How much money is an additional RCS reduction of a few percent worth?

Maintenance and Testing. A second important cost driver is the maintenance of an LO platform. The natural elements, along with the harsh operating environment, stress and degrade the electrical and mechanical properties of materials. Special testing methods are required to determine if and when the RCS has been affected by exposure to the environment. So-called go–no-go tests compare a set of measured data from the platform under test with a reference data set obtained from a known "clean" one of identical configuration. A significant deviation in the data sets would signify a correspondingly significant change in RCS. A test of this type does not require a high level of precision, and therefore can be conducted using portable test equipment. Data can be taken by probes located close to the platform surfaces, that is, in the near-field region of the scatterers.

If a platform fails the go–no-go check in the field, then it will be sent to a test and repair facility for further evaluation. Specialized facilities and repair techniques are required because of the uncommon materials involved and the exacting tolerances that must be satisfied. The integrity of localized repairs can be checked using hand-held reflection devices that verify local surface reflection characteristics.

Tradeoff between Stealth and Electronic Warfare. Low observability demands the most of technology and forces concessions in many other aspects of platform design and performance. At some point the burden of increasing stealth may become unacceptable. Electronic warfare (*EW*) techniques (now referred to as *electronic attack* and *electronic protect* in the United States) are a complement to low RCS. Common EW techniques currently in use around the world include jamming, decoys, and chaff (22). The major disadvantage of EW is that the radar is aware of the target's presence. However, the radar is denied information on the target's range and velocity. Even though the radar is not completely disabled, a combination of EW and low RCS can cause the radar to loose lock, forcing it to reacquire a target repeatedly. This is a time-consuming process that ties up valuable radar resources. With all other factors constant, chaff, deception, and jamming are more effective for low-RCS targets than for conventional ones.

Some older platforms currently in the field are being retro-fitted or upgraded to reduce the RCS and other signatures. All new aircraft, ships, and ground vehicles are incorporating some degree of stealth design and technology. However, it appears that the complete dominance of stealth in all aspects of design, as seen in the F-117, has been abandoned. Programs like the F-22, the Comanche helicopter, and the Euro-fighter are opting for a balance between stealth and other performance measures.

The Radar Equation

Consider the situation shown in Fig. 1 with the radar operating at a frequency f. The corresponding wavelength is $\lambda = c/f$, where $c \approx 2.998 \times 10^8$ m/s is the speed of light in free space. Define the following quantities: where

P_t = transmitter power delivered to the transmit antenna

G_t = transmit antenna gain, a measure of how efficiently the antenna concentrates power in the direction of the target

G_r = receive antenna gain

A_{er} = effective area of the receive antenna, which can approach the physical area of the antenna aperture for a very efficient antenna

From antenna theory, antenna gain and effective area are related by

$$G_r = \frac{4\pi A_{er}}{\lambda^2} \tag{11}$$

The power scattered by the target that is delivered to the receive antenna terminals is given by

$$P_r \frac{P_t G_t}{4\pi R_t^2} \sigma \frac{1}{4\pi R_r^2} A_{er}$$

The first factor on the right-hand side is the power density incident on the target. Multiplying this factor by σ gives the fraction of incident power scattered in the direction of the receiver. The product of the first three factors represents the scattered power density at the receive antenna. Finally, multiplying by A_{er} gives the scattered power collected by the antenna.

Specializing to the monostatic case ($G_t = G_r \equiv G$ and ($R_t = R_r \equiv R$) and using the relationship between effective area and gain give the result

$$P_r = \frac{P_t G^2 \sigma \lambda^2}{(4\pi)^3 R^4}$$

This form of the radar equation is too simple to be of practical use in predicting a radar's performance. However, two important features are evident. The first is the R^4 in the denominator, which is a disadvantage to the radar system designer, whose goal is to increase the detection range of the radar. The second is that the received power is linearly related to σ, which is a disadvantage to the RCS engineer.

If the minimum scattered power that the radar receiver can detect is P_m, then the corresponding maximum detection range is obtained by solving the radar equation for R:

$$R_m = \sqrt[4]{\frac{P_t G^2 \sigma \lambda^2}{(4\pi)^3 P_m}} \tag{12}$$

Therefore, to halve the maximum detection range requires that the RCS be reduced by a factor of 2^4 (=16).

Finally, note that the radar equation was derived for a single-frequency wave. Typical radar waveforms, such as pulse trains, occupy a band of frequencies. The radar equation may have to be evaluated at several frequencies in the radar band if the quantities in the equation are not constant.

Calculation of Radar Cross Section

RCS prediction methods can be broadly categorized as either rigorous or approximate. Rigorous methods are those that have been shown by mathematical proof to converge to the exact result under the appropriate conditions. However, in practice, there is always some small error present in the computed data due to the numerical evaluation of integrals, computer roundoff, and so on. Examples of rigorous methods are the finite-difference time domain (*FDTD*) technique and the MM.

Approximate formulations are based on assumptions and therefore are subject to limitations in their application and accuracy. Unlike the rigorous methods, even if there is no computational error, the approximate result will not necessarily converge to the true result. If the approximation is a good one, then the error will not be significant for the problem under consideration. Examples of approximate methods are PO and microwave optics.

Phasors. Phasor notation is commonly used when working with time-harmonic fields. *Time-harmonic fields* are those that have a sinusoidal time variation of the form $\cos \omega t$, where $\omega = 2\pi f$. Since the sources and fields have the same time dependence, it can be factored out of all electromagnetic quantities and suppressed (i.e., dropped). When the calculations are completed, the time variation is reintroduced. Thus a time-varying quantity $\boldsymbol{E}(x, y, z, t)$ can be obtained from the phasor $\boldsymbol{E}(x, y, z)$ by multiplying the phasor by $e^{j\omega t}$ and taking the real part

$$\boldsymbol{\mathcal{E}}(x, y, z, t) = \mathrm{Re}[\boldsymbol{E}(x, y, z)e^{j\omega t}]$$

All quantities appearing throughout this article are phasors unless otherwise indicated.

Spherical and Plane Waves. Ideal spherical waves (i.e., waves for which the planes of constant phase are spheres) originate from point sources, which do not actually exist. However, for practical purposes, spherical wave behavior results if the observer is located "far enough" from an extended source as depicted in Fig. 1. Spherical waves have the phasor form

$$\boldsymbol{E}(r) = \boldsymbol{E}_0 \frac{e^{-j\beta r}}{r} \tag{13}$$

where r is the distance from the source. The vector constant $\boldsymbol{E}_0$ (which may have complex components) is determined by the amplitude, phase, and polarization of the extended source.

At great distances from the source ($r \to \infty$) the target only intercepts a small section of the spherical wave front with a very large radius of curvature. Thus it appears that planes of constant phase exist over the extent of the target, and the electric field can be approximated by

$$\boldsymbol{E}(r) = \boldsymbol{E}_0 e^{-j\beta r}$$

where r is now the distance from the phase reference and $\boldsymbol{E}_0$ is determined from the intensity of the spherical wave at the target. If the source is at the origin of a spherical coordinate system, then $\boldsymbol{E}_0$ can only have $\hat{\theta}$ and $\hat{\Phi}$ components in the far zone. (This would be the case for a radar antenna located at the origin.)

Both spherical and plane waves have the characteristics of a transverse electromagnetic (TEM) wave:

(1) The electric and magnetic field vectors are perpendicular to each other and the direction of propagation.
(2) The magnitudes of the electric and magnetic fields are related by the intrinsic impedance of free space.

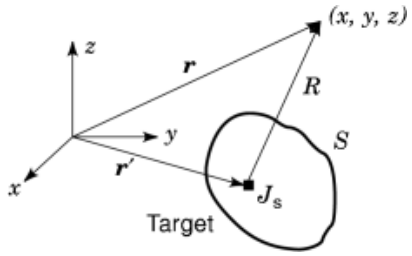

Fig. 9. Current flows on the surface of a PEC. The total scattered field at the observation point is obtained by an integration of the current over the entire surface.

Thus, if $\hat{\beta}$ is a unit vector in the direction of propagation,

$$\boldsymbol{H} = \frac{\hat{\boldsymbol{\beta}} \times \boldsymbol{E}}{\eta_0} \tag{14}$$

A plane wave of arbitrary polarization is given by the formula

$$\boldsymbol{E} = (E_{0\theta}\hat{\boldsymbol{\theta}} + E_{0\phi}\hat{\boldsymbol{\phi}})e^{-j\boldsymbol{\beta}\cdot\boldsymbol{r}} \tag{15}$$

where **r** is a position vector to the point x, y, z at which the field is to be evaluated:

$$\boldsymbol{r} = \hat{\boldsymbol{x}}x + \hat{\boldsymbol{y}}y + \hat{\boldsymbol{z}}z$$

The corresponding magnetic field intensity for a plane wave propagating inward toward the origin ($\hat{\beta} = -\hat{r}$) is

$$\boldsymbol{H} = -\frac{1}{\eta_0}(E_{0\theta}\hat{\boldsymbol{\phi}} - E_{0\phi}\hat{\boldsymbol{\theta}})e^{-j\boldsymbol{\beta}\cdot\boldsymbol{r}} \tag{16}$$

The $\hat{\theta}$ component of the electric field is called *transverse magnetic to z* (TM_z) because the magnetic field vector associated with this component [$E_{0\theta}\hat{\phi}$ term in Eq. (16)] lies entirely in a plane transverse to the z axis. Similarly, the $\hat{\Phi}$ component of the electric field is referred to as *transverse electric to z* (TE_z) because this component of the electric field [$E_{0\phi}\hat{\phi}$ term in Eq. (15)] lies entirely in a plane transverse to the z axis. Thus, for a TM_z-polarized plane wave $E_{0\phi} = 0$; for a TE_z-polarized plane wave $E_{0\theta} = 0$. Any arbitrary polarization can be expressed as a linear combination of the two. In a similar manner one could define TE_x, TM_y, and so on.

Radiation Integrals. Scattered fields are set up by a combination of electric and (in general) magnetic currents. Currents are induced such that the total fields satisfy the boundary conditions and Maxwell's equations. The radiation integrals provide a means of calculating the fields due to a prescribed set of currents. The radiation integrals, or Stratton–Chu integrals, are integral solutions to Maxwell's equations. They can be derived directly by taking the curl of Maxwell's first two equations, using the vector Green's theorem, and then integrating (23).

For RCS calculations, according to Eq. (1), only the scattered field far from the target is of interest, because $R \to \infty$. Consider a scattering body of volume V that is enclosed by a surface S as shown in Fig. 9. The standard convention is to denote observation point quantities by unprimed symbols, and source point quantities by primed symbols.

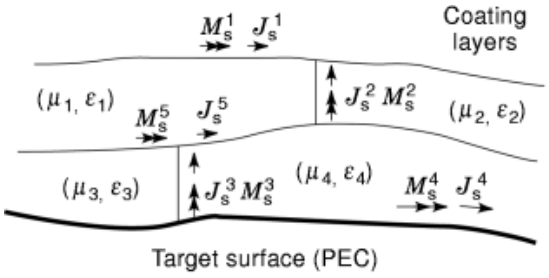

Fig. 10. If a target is not a PEC, then volume currents may exist inside of the target. The volume currents can be replaced by surface currents using the surface equivalence principle.

In the far zone, the following approximations are employed:

(1) The vector from the origin to the observation point and the vector from any source point on S to the observation point are approximately parallel ($\boldsymbol{R}$ parallel to $\boldsymbol{r}$).
(2) For large distances the difference in amplitude between a spherical wave emanating from the origin and one emanating from any point on the surface S is negligible ($1/R \approx 1/r$).

With these assumptions, the radiation integral for the electric field components tangential to a sphere of radius r centered at the origin can be expressed as

$$\boldsymbol{E}_{s\theta}(x,y,z) = -\frac{j\beta\eta_0}{4\pi r}\, e^{-j\beta r} \iiint_V \left(\boldsymbol{J}\cdot\hat{\boldsymbol{\theta}} + \frac{1}{\eta_0}\boldsymbol{M}\cdot\hat{\boldsymbol{\phi}}\right) e^{-j\beta\hat{\boldsymbol{r}}\cdot\boldsymbol{r}'} \tag{17a}$$

$$\boldsymbol{E}_{s\phi}(x,y,z) = -\frac{j\beta\eta_0}{4\pi r}\, e^{-j\beta r} \iiint_V \left(\boldsymbol{J}\cdot\hat{\boldsymbol{\phi}} - \frac{1}{\eta_0}\boldsymbol{M}\cdot\hat{\boldsymbol{\theta}}\right) e^{-j\beta\hat{\boldsymbol{r}}\cdot\boldsymbol{r}'} \tag{17b}$$

where $\boldsymbol{J}$ (A/m^2) and $\boldsymbol{M}$ (V/m^2) are the volume electric and magnetic currents, respectively. (Magnetic current is a fictitious quantity because isolated magnetic charge does not exist, but under some circumstances it is used as a matter of mathematical convenience.)

The use of volume current is advantageous for computing the scattered fields from highly inhomogeneous bodies. However, for most targets, it is more efficient to use a surface current formulation. As shown in Fig. 10, current flows on all interfaces between materials, as well as the external surface of the target. For surface currents, the far-field form of the radiation integral becomes

$$\boldsymbol{E}_{s\theta}(x,y,z) = -\frac{j\beta\eta_0}{4\pi r}\, e^{-j\beta r} \iint_S \left(\boldsymbol{J}_s\cdot\hat{\boldsymbol{\theta}} + \frac{1}{\eta_0}\boldsymbol{M}_s\cdot\hat{\boldsymbol{\phi}}\right) e^{-j\beta\hat{\boldsymbol{r}}\cdot\boldsymbol{r}'} \tag{18a}$$

$$\boldsymbol{E}_{s\phi}(x,y,z) = -\frac{j\beta\eta_0}{4\pi r}\, e^{-j\beta r} \iint_S \left(\boldsymbol{J}_s\cdot\hat{\boldsymbol{\phi}} - \frac{1}{\eta_0}\boldsymbol{M}_s\cdot\hat{\boldsymbol{\theta}}\right) e^{-j\beta\hat{\boldsymbol{r}}\cdot\boldsymbol{r}'} \tag{18b}$$

where S includes all of the surfaces over which nonzero current exists. If the current is known, then the integrals in Eqs. (17) or (18) can be evaluated numerically.

Table 3. Summary of Approximate Methods For RCS Prediction

Mechanism	Current Based	Ray Optics Based
Surface scattering	GO surface current–physical optics (PO)	Specular rays–geometrical optics (GO)
Edge scattering	Fringe currents–physical theory of diffraction (PTD)	Diffracted rays–geometrical theory of diffraction (GTD)
Surface waves	Interaction between fringe currents	Multiple diffractions between edges

If the scattering body is a perfect electrical conductor (*PEC*), then only electric current exists, and the surface of integration corresponds to a real physical surface. However, S in Eq. (18) need not exist; it can be a fictitious surface defined for convenience. The currents on the fictitious surface can be determined from the actual tangential electric and magnetic fields at every point on S. Thus

$$\boldsymbol{J}_S = \hat{\boldsymbol{n}} \times \boldsymbol{H} \tag{19a}$$

$$\boldsymbol{M}_S = \hat{\boldsymbol{n}} \times \boldsymbol{E} \tag{19b}$$

where $\hat{n}$ is the unit vector normal to the surface. This is a consequence of the *equivalence principle* of electromagnetics (4).

Approximate Prediction Methods. Approximate prediction methods are used for a variety of reasons, but primarily because they are computationally less demanding, thereby allowing data to be generated more rapidly. This is an advantage in the early stages of design, when major tradeoff studies are being performed. Coarse approximations can be applied in the beginning, and then refined as the design progresses. Eventually it may be necessary to verify the performance of a specific design by a rigorous calculation.

At microwave frequencies, useful approximations should include scattering contributions from large surface areas, edges, surface waves, and interactions between and among surfaces and edges. There are two approaches to computing the RCS. One is based on estimating the induced currents and is referred to as a current-based approach: the PO approximation. The second is based on postulating relationships between the incident and scattered waves, or rays: GO. This is a ray-based approach.

PO and GO are used to calculate the scattered field from surfaces; the effects of the edges of surfaces are not properly modeled or not included. Supplemental theories have been developed to allow for edge scattering. The PTD is the current-based method used in conjunction with PO. The GTD is a ray-based method for calculating diffracted fields. Both the current and ray approaches can be shown to yield identical results under the same conditions. Table 3 summarizes the two methods.

Physical Optics. A rigorous calculation of the currents $\boldsymbol{J}_s$ and $\boldsymbol{M}_s$ typically requires a great amount computational effort. The PO approximation is an estimate of the electric current that is accurate for a large,

smooth PEC. The current is approximated by (9)

$$\boldsymbol{J}_S(x,y,z) = \begin{cases} 2\hat{\boldsymbol{n}}(x,y,z) \times \boldsymbol{H}_i(x,y,z) \\ \qquad\qquad \text{on the illuminated part of } S \\ 0 \qquad\qquad \text{on the shadowed part of } S \end{cases} \tag{20}$$

where $\boldsymbol{H}_i$ is the incident magnetic field intensity.

Equation (20) is explained by approximating the target surface in the vicinity of the point (x, y, z) by an infinite, flat surface. Assume that the incident wave is due to a source at a distance R and the electric field vector is parallel to the surface. By the method of images, the target can be removed and replaced by an equivalent scattering source at a distance R below the surface. To satisfy the boundary conditions (i.e., the tangential component of the total electric field must be zero) the electric field of the equivalent scattering source must be equal and opposite to that of the incident field. Because the two waves are propagating in opposite directions toward the surface, from Eq. (14) the magnetic field vectors will be oriented in the same direction. Thus the factor of 2 in Eq. (20).

Perhaps the simplest application of the PO approximation is for a flat plate (6). Let the plate be centered at the origin in the $z = 0$ plane and have dimensions of a in the x direction and b in the y direction. A plane wave of arbitrary polarization is incident at an angle an angle θ_i. The PO approximation for the current is

$$\boldsymbol{J}_S \approx 2(J_{0x}\hat{\boldsymbol{x}} + J_{0y}\hat{\boldsymbol{y}}) \frac{e^{-j\beta \hat{\boldsymbol{r}}_i \cdot \boldsymbol{r}'}}{\eta_0} \tag{21}$$

where

$$J_{0x} = E_{0\theta} \cos\phi - E_{0\phi} \cos\theta \sin\phi$$
$$J_{0y} = E_{0\theta} \sin\phi + E_{0\phi} \cos\theta \cos\phi$$

and

$$-\hat{\boldsymbol{r}}_i \cdot \boldsymbol{r}' = u_i x + v_i y + w_i z$$

The subscript i denotes incident wave quantities. The x, y, and direction cosines are defined by

$$u_i = \sin\theta_i \cos\phi_i \tag{22a}$$
$$v_i = \sin\theta_i \sin\phi_i \tag{22b}$$
$$w_i = \cos\theta_i \tag{22c}$$

Using Equation (21) in 18a and the fact that $z' = 0$ gives

$$E_{s\theta} = \frac{-j\beta}{2\pi r} e^{-j\beta r} \hat{\boldsymbol{\theta}} \cdot (J_{0x}\hat{\boldsymbol{x}} + J_{0y}\hat{\boldsymbol{y}}) \int_{-a/2}^{a/2} \int_{-b/2}^{b/2} e^{j\beta(x'u_i + y'v_i)} e^{j\beta(x'u + y'v)}\, dx'\, dy' \tag{23}$$

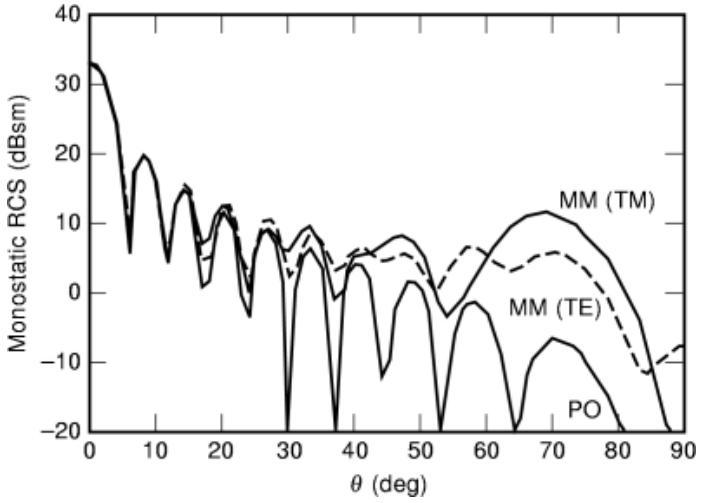

Fig. 11. A comparison of the RCS of a plate with dimensions $a = 5\lambda$ and $b = 2.5\lambda$ in the plane $\phi = 0^\circ$. The approximate (PO) and rigorous (MM) methods are in close agreement in the region of the main lobe but disagree at wide angles.

For the monostatic RCS $u_i = u$ and $v_i = v$; therefore the exponents in the integrand can be combined. Furthermore, the x and y integrals can be separated, and both are of the form

$$\int_{-a/2}^{a/2} e^{j2\beta x' u}\, dx' = a\frac{\sin(\beta u a)}{\beta u a} \equiv a\,\mathrm{sinc}(\beta u a) \qquad (24)$$

Now assume that a TM_z-polarized plane wave is incident ($E_{0\phi} = 0$) and the radar receive antenna is sensitive to the same polarization. Thus we use the notation $\sigma_{\theta\theta}$ where the first subscript denotes the polarization of the receiver and the second the polarization of the incident wave. Using Eqs. (23) and (24) in the definition of RCS yields

$$\sigma_{\theta\theta} = \frac{4\pi A^2}{\lambda^2}\,\mathrm{sinc}^2(\beta u a)\,\mathrm{sinc}^2(\beta v b)\cos^2\theta \qquad (25)$$

where $A = ab$ is the area of the plate.

The monostatic RCS of a square plate with $a = 5\lambda$ and $b = 2.5\lambda$ is shown in Fig. 11 for $\phi = 0^\circ$. The xz and yz planes are referred to as *principal planes,* because they are transverse to the plate edges. For comparison, the RCS obtained by a rigorous calculation of the current (MM) is also shown. (The MM result is converged and can therefore be considered exact.) The maxima of the sinc(·) functions in Eq. (25) occur at $\theta = \phi = 0^\circ$ and have values of 1. Thus the maximum value of the RCS is given by Eq. (6). As the dimensions of the plate in wavelengths increase, the width of the central lobe narrows. Note that the major difference between the two methods occurs at wide angles (near $\pm 90^\circ$). In this region the RCS is primarily determined by the current distribution near the plate edges, which is where the PO approximation fails.

Physical Theory of Diffraction. The PTD, also known as the method of edge waves (*MEW*), is a current-based approach to obtaining the edge scattered field (24). The total current on a conductor with an edge can be decomposed into a PO component and a nonuniform (edge or fringe) component. If the fringe current is known,

then the edge-scattered field can be computed by using this current in the radiation integral. The total field at an observation point is the sum of the PO and edge-scattered fields.

For a surface that is very large relative to the wavelength of the incident wave, the current distribution at a point near the edge is primarily determined by the local features of the geometry. If the edge is very long and the point under consideration is not close to the end of the edge, then the current is approximately the same as that for an infinitely long edge. Thus edge scattering can be considered a local phenomenon, and the current approximated by the current of the corresponding canonical scattering problem. (A canonical problem is one that has fundamentally the same geometry as the one under consideration, but whose solution is known.) If the total current can be determined for a canonical problem, in this case an infinite knife edge, then the PO component can be subtracted out and the result used as an estimate for the fringe current on a finite edge. The fringe currents are then used in the radiation integrals to obtain an edge-scattered field.

This approach has the advantage that the edge-scattered fields remain finite at shadow and reflection boundaries. However, the fringe currents extend a significant distance from the edge (a minimum of about 0.5λ), so that two-dimensional integrals must be evaluated. Michaeli has reduced the PTD fringe currents to filaments that flow along the body edge, thus reducing the integration to one dimension (25).

The electric and magnetic current filaments for a knife edge are given by

$$I_e = \frac{-2j}{\eta_0 \beta \sin^2 \gamma'} \frac{\sqrt{2}\sin(\phi'/2)}{\cos\phi' + \delta}[\sqrt{1-\delta} - \sqrt{2}\cos(\phi'/2)](\boldsymbol{E}_i)_{\tan} + \frac{2j}{\beta \sin\gamma' (\cos\phi' + \delta)} \left(\cot\gamma' \cos\phi' + \cos\phi \cot\gamma + \sqrt{2}\cos(\phi'/2) \frac{\delta \cot\gamma' - \cot\gamma \cos\phi}{\sqrt{1-\delta}} \right) (\boldsymbol{H}_i)_{\tan} \quad (26)$$

$$I_m = \frac{2j\eta_0}{\beta \sin\gamma' \sin\gamma \cos\phi' + \delta} \left(1 - \frac{\sqrt{2}\cos(\phi'/2)}{\sqrt{1-\delta}} \right) (\boldsymbol{H}_i)_{\tan} \quad (27)$$

where

$$\delta = \frac{\cos\gamma' \cos\gamma + \sin\gamma' \sin\gamma - \cos^2\gamma'}{\sin^2\gamma'}$$

The PTD is simple in principle, but can be inconvenient in practice. The currents in Eqs. (26) and (27) are a function of incidence angle, so for monostatic calculations the integrations must be performed again after each angle change. Another disadvantage is that modeling the fringe current interaction is difficult. On the plus side is that the edge-scattered field is simply added to the PO field. This is the major attraction of the PTD, since PO is so convenient and widely used.

Geometrical Optics. GO is the theory of ray tracing that has been used for centuries to design systems of lenses such as telescopes. It works well at optical frequencies because the lens and mirror dimensions are much larger than a wavelength and thus the interaction of the wave with the lens becomes a localized phenomenon. The reflected ray appears to originate from a single point on the surface, called a specular or reflection point.

GO is the most basic theory that describes wave behavior upon reflection or refraction at an interface between two materials (10). GO is based on seven assumptions or postulates:

(1) Waves are everywhere locally plane and TEM.

(2) The wave direction is specified by the normal to the equiphase surfaces, that is, a ray. (Equiphase surfaces are also referred to as eikonal surfaces.)
(3) Rays travel in straight lines in a homogeneous medium (Fermat's principle).
(4) Polarization is constant along a ray.
(5) At the reflection point, the reflected fields are linearly related to the incident fields by reflection coefficients.
(6) Reflected rays satisfy the law of reflection.
(7) Power in a tube of rays is conserved. The field strength is inversely proportional to the square root of the cross-sectional area of the flux tube.

Ray tubes are also called ray bundles or flux tubes. For a plane wave, all of the rays are parallel and therefore a bundle of rays has a constant cross section. However, for a spherical wave, a bundle of rays expands as the distance from the source increases. The power flowing through a slice of the bundle must be constant if the medium is lossless and power is conserved.

For the general scattering problem the incident wave front and scattering surface may have some curvature, as illustrated in Fig. 12. The local curvature at a point on a doubly curved surface, whether it is a wave front or target surface, can be expressed in terms of two principal radii of curvature. Let the incident wave front be characterized by the principal radii of curvature $R^{\mathrm{i}}{}_1$ and $R^{\mathrm{i}}{}_2$. Similarly, let the scattering surface be characterized by the principal radii of curvature $R^{\mathrm{s}}{}_1$ and $R^{\mathrm{s}}{}_2$. If these two sets of radii are known, then the radii of curvature of the reflected wave front can be computed using the following equation:

$$\frac{1}{R^{\mathrm{r}}_{1,2}} = \frac{1}{2}\left(\frac{1}{R^{\mathrm{i}}_1} + \frac{1}{R^{\mathrm{i}}_2}\right) + \frac{1}{f_{1,2}} \tag{28}$$

where $f_{1,2}$ are the focal lengths in the two principal planes. (The focal length is another measure of curvature.) The focal lengths can be computed by (4)

$$\frac{1}{f_{1,2}} = \frac{1}{\cos\theta_{\mathrm{i}}}\left(\frac{\sin^2\theta_2}{R^{\mathrm{s}}_1} + \frac{\sin^2\theta_1}{R^{\mathrm{s}}_2}\right) \pm \left[\frac{1}{\cos^2\theta_{\mathrm{i}}}\left(\frac{\sin^2\theta_2}{R^{\mathrm{s}}_1} + \frac{\sin^2\theta_1}{R^{\mathrm{s}}_2}\right)^2 - \frac{4}{R^{\mathrm{s}}_1 R^{\mathrm{s}}_2}\right]^{1/2} \tag{29}$$

where the angles are given by

$$\theta_1 = \cos^{-1}(\hat{\boldsymbol{t}}_1 \cdot \hat{\boldsymbol{\beta}}_{\mathrm{i}}) \tag{30a}$$
$$\theta_2 = \cos^{-1}(\hat{\boldsymbol{t}}_2 \cdot \hat{\boldsymbol{\beta}}_{\mathrm{i}}) \tag{30b}$$
$$\theta_{\mathrm{i}} = \cos^{-1}(\hat{\boldsymbol{n}} \cdot \hat{\boldsymbol{\beta}}_{\mathrm{i}}) \tag{30c}$$

The vectors $\hat{I}_1$ and $\hat{t}_2$ are tangent to the surface at the reflection point and lie in principal planes 1 and 2, respectively.

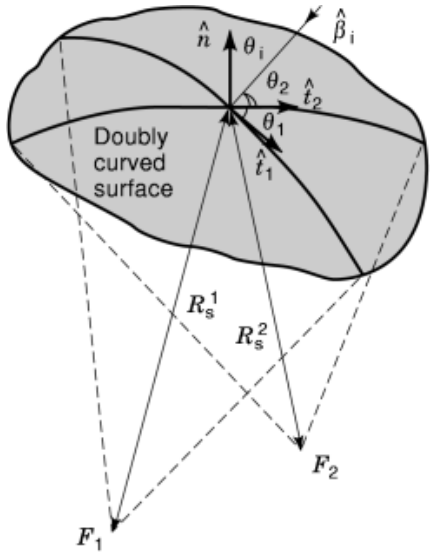

Fig. 12. GO can be used to predict the reflected field from a doubly curved surface. The curvatures of the incident wave front and surface affect the curvature of the reflected wave front.

The postulates allow the reflected field to be computed from the incident field at the reflection point by multiplying by a reflection coefficient. In matrix form,

$$\boldsymbol{E}_r(s) = \boldsymbol{R} \cdot \boldsymbol{E}_i(s')A(s)e^{-j\beta s}e^{j\phi_c} \tag{31}$$

where

$$\boldsymbol{E}_r(s) = \begin{bmatrix} E_{r\perp}(s) \\ E_{r\parallel}(s) \end{bmatrix} \tag{32}$$

$$\boldsymbol{E}_i(s') = \begin{bmatrix} E_{i\perp}(s') \\ E_{i\parallel}(s') \end{bmatrix} \tag{33}$$

and the reflection coefficient matrix is

$$\boldsymbol{R} = \begin{bmatrix} \Gamma_{\perp\perp} & \Gamma_{\perp\parallel} \\ \Gamma_{\parallel\perp} & \Gamma_{\parallel\parallel} \end{bmatrix} \tag{34}$$

The subscripts $\parallel$ and $\perp$ refer to a polarization where the electric field is parallel or perpendicular to the plane of incidence (the plane defined by the vectors $\hat{I}$ and $\hat{\beta}_i$).

The divergence and spreading factor for the reflected wave is

$$A(s) = \left(\frac{R_1^r R_2^r}{(R_1^r + s)(R_2^r + s)} \right)^{1/2} \tag{35}$$

The quantity s' is the distance from the source point S to the reflection point Q, and s is the distance along the reflected ray from the reflection point to the observation point P.

The last factor in Eq. (31) allows for phase transitions through caustics, which are points or lines at which the cross section of a ray tube is zero (and thus the power density is infinite); we have

$$\phi_c = \begin{cases} 0 & \text{if neither center of curvature lies between } Q \text{ and } P \\ \pi/2 & \text{if one center of curvature lies between } Q \text{ and } P \\ \pi & \text{if both centers of curvature lies between } Q \text{ and } P \end{cases} \tag{36}$$

A well-known formula for the RCS of a curved surface can be derived using the above formulas. The fact that for a plane wave $R^i{}_1 = R^i{}_2 = \infty$ and the observer is far from the target ($R^s{}_1$, $R^s{}_2 \gg s$) yields the approximation

$$\sigma \approx \pi R_1^s R_2^s \tag{37}$$

Equation (37) has been widely applied to basic geometric shapes such as spheres and ellipsoids. Note that GO predicts zero field in shadow regions. That is, if the path between the source and observation points is blocked, then there is no received field.

Geometrical Theory of Diffraction. GO provides a means of calculating the field reflected from a surface. The associated edge effects require a mathematical model for edge diffraction. The GTD is such a ray-based edge diffraction theory (26). For the GTD, rays are hypothesized that obey diffraction laws similar to reflection laws. A diffraction coefficient is defined, which depends on the edge geometry and polarization of the incident wave. Upon diffraction, the scattered field is given by the incident field times the diffraction coefficient. Furthermore, the diffracted wave follows prescribed straight line paths in free space. The total field at an observation point is the vector sum of all the reflected and diffracted fields arriving at that point.

As first developed, the GTD had several shortcomings with regard to singularities in the field. Several modified versions of the GTD, such as the uniform theory of diffraction (*UTD*) (27) and the asymptotic theory of diffraction (*ATD*) (28), have eliminated the problems in many cases by introducing correction factors. In the following discussions GTD will refer to the collection of these diffraction theories.

The postulates of the GTD are similar to those of GO; only numbers 5 and 6 change:

(1) At the diffraction point, the diffracted fields are linearly related to the incident fields by diffraction coefficients.
(2) Diffracted rays emerge radially from the edge.

In addition, rays traversing a caustic encounter a phase advance of 90°; an edge is always a caustic. At a focus there is a phase advance of 180°.

The behavior of diffracted rays from an infinite conducting wedge is illustrated in Fig. 13. The diffracted rays lie on the surface of a cone (referred to as the Keller cone) with its tip located at the diffraction point and

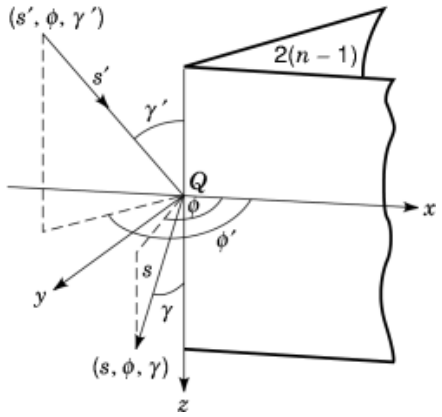

Fig. 13. The GTD is used to predict edge diffracted fields. As long as the diffraction point is not near the end of the edge, the diffracted field is similar to that of an infinitely long edge.

axis along the edge. The cone half angle γ is equal to the angle that the incident ray makes with the edge, γ' (a consequence of Fermat's principle). The coordinate variables (s, γ, ϕ) and (s', γ', ϕ') uniquely define the directions of diffraction (observation) and incidence (source), respectively.

In the light of postulate 5 the diffracted field from an edge can be written as

$$\boldsymbol{E}_{\mathrm{d}}(s) = \boldsymbol{D} \cdot \boldsymbol{E}_{\mathrm{i}}(s') A(s) e^{-j\beta s} \tag{38}$$

The vectors $\boldsymbol{E}_{\mathrm{d}}$ and $\boldsymbol{E}_{\mathrm{i}}$ have the same form as in Eq. (32) and Eq. (33), except that parallel and perpendicular are defined relative to the edge rather than the plane of incidence. In Eq. (38) $\boldsymbol{D}$ is a two-dimensional matrix of diffraction coefficients,

$$\boldsymbol{D} = \begin{bmatrix} D_{\perp\perp} & D_{\perp\parallel} \\ D_{\parallel\perp} & D_{\parallel\parallel} \end{bmatrix} \tag{39}$$

and the divergence and spreading factor is

$$A(s) = \left(\frac{\rho_{\mathrm{c}}}{s(\rho_{\mathrm{c}} + s)} \right)^{1/2} = \begin{cases} \dfrac{1}{\sqrt{s}}, & \text{plane waves} \\ \sqrt{\dfrac{s'}{s(s+s')}}, & \text{spherical waves} \end{cases} \tag{40}$$

where ρ_{c} is the distance from the caustic.

The diffraction coefficients are derived from the appropriate canonical problem. The GO field is subtracted from the total scattered field. The difference is the diffracted field, which can be used to determine the elements of $\boldsymbol{D}$, given the known form of Eq. (36). For a knife edge the diffraction coefficients are

$$D_{\parallel,\perp} = \frac{e^{-j\pi/4}}{2\sqrt{2\pi\beta}\sin\gamma} \left(\frac{F\left(\beta \ell a(\phi^-)\right)}{\cos\phi^-} \pm \frac{F\left(\beta \ell a(\phi^+)\right)}{\cos\phi^+} \right) \tag{41}$$

where the transition function is

$$F(\xi) = j2|\sqrt{\xi}|e^{j\xi}\int_{|\sqrt{\xi}|}^{\infty} e^{-j\tau^2}\,d\tau \qquad (42)$$

with

$$\phi^{\pm} = \phi \pm \phi'$$
$$a(\phi^{\pm}) = 2\cos(\phi^{\pm}/2)$$

$$\ell = \begin{cases} \dfrac{ss'}{s+s'}\sin^2\gamma, & \text{spherical waves} \\ s\sin^2\gamma, & \text{plane waves} \end{cases} \qquad (43)$$

In special cases where $\boldsymbol{E}_{\mathrm{d}}$ is tangent to the surface of a PEC, the surface diffracted ray is zero. For a rectangular plate, there will not be an interaction (higher-order diffraction) between the two parallel edges. In fact, there is an interaction between two edges of a parallel plate even when the electric field is parallel to the edge, and it is included by adding a slope diffraction term to Eq. (38)

$$\boldsymbol{E}_{\mathrm{d}}(s) = \left(\boldsymbol{D}\cdot\boldsymbol{E}_{\mathrm{i}}(Q) + \boldsymbol{D}'\cdot\left.\frac{\partial\boldsymbol{E}_{\mathrm{i}}}{\partial n}\right|_{Q}\right)A(s)e^{-j\beta s} \qquad (44)$$

where $\boldsymbol{D}'$ is a matrix of slope diffraction coefficients.

Rigorous Methods.

Method of Moments. The radiation integrals provide a means of calculating the scattered field from a target once the induced current on the surface is known. Except for the most simple shapes, the current distribution on the target is not known accurately. For electrically large bodies that are smooth and sufficiently flat, the PO approximation provides a good estimate at points far from discontinuities and shadow boundaries. By a discontinuity is meant any abrupt change in the surface contour or composition. Examples are edges, steps, cracks, and material joints.

In order to compute the current rigorously, an integral equation (IE) for the current can be formulated from Maxwell's equations and the boundary conditions. IEs have the unknown quantity in the integrand and possibly in other terms outside of the integral. In most problems of practical interest, the IE must be solved numerically using a computer. The most popular solution technique, called the *method of moments* (MM), consists in expanding the current into a series with unknown coefficients (11). The expansion is inserted into the integral equation and a weighting process applied. The properties of the expansion functions are used to reduce the integral equation to a set of simultaneous linear equations that can be solved for the coefficients.

The E-field integral equation (EFIE) is the most commonly used. It can be derived by using the general form of the radiation integrals and placing the observation point on the surface of the body. [The general form of the radiation integrals does not make the assumption of a far-field observation point as in Eqs. (17) and (18).] If the target is a PEC, then $(\boldsymbol{E}_{\mathrm{i}} + \boldsymbol{E}_{\mathrm{s}})_{\tan} = 0$ on the surface. The incident field is known, and the radiation integrals give the scattered field in terms of the unknown surface current. Thus the following form of the EFIE

is obtained:

$$\boldsymbol{E}_{\mathrm{i}}(\boldsymbol{r})\Big|_{\tan} = \iint_S \Big(j\omega\mu_0 \boldsymbol{J}_{\mathrm{s}}(\boldsymbol{r}')G(\boldsymbol{r},\boldsymbol{r}') - \frac{j}{\omega\epsilon}[\nabla' \cdot \boldsymbol{J}_{\mathrm{s}}(\boldsymbol{r}')][\nabla' G(\boldsymbol{r}')] \Big)_{\tan} ds' \tag{45}$$

where, as usual, primes denote source point quantities associated with the current and unprimed denotes observation point quantities. The free space Green's function is defined by

$$G(\boldsymbol{r},\boldsymbol{r}') = \frac{e^{-j\beta R(\boldsymbol{r},\boldsymbol{r}')}}{4\pi R(\boldsymbol{r},\boldsymbol{r}')} \tag{46}$$

with

$$R(\boldsymbol{r},\boldsymbol{r}') = \sqrt{(x-x')^2 + (y-y')^2 + (z-z')^2}$$

Equation (45) is reduced to a matrix equation using the MM. First the current is expanded into a series of basis functions $\{\boldsymbol{J}_n\}$ with unknown current coefficients $\{I_n\}$:

$$\boldsymbol{J}_{\mathrm{s}}(\boldsymbol{r}') = \sum_{n=1}^{N} I_n \boldsymbol{J}_n(\boldsymbol{r}') \tag{47}$$

The basis functions are chosen to be mathematically convenient and adequately represent the current over the surface. They are of two general types: (1) subdomain or (2) entire domain. In the subdomain case, each function is nonzero over only a part of the surface. On the other hand, each entire-domain basis function is nonzero over the entire surface. Using a function of time as an analogy, it can be expressed as a series of sinusoids (Fourier series), which are an example of entire-domain basis functions. The time function could also be expressed as a series of steps (a "stair step" approximation), which is an example of subdomain basis functions.

Once the basis functions are chosen, Eq. (47) is inserted into Eq. (45) and a test is performed that involves multiplying by a set of weighting functions $\boldsymbol{W}_n$ and integrating. Generally the complex conjugates of the basis functions are selected as the weighting functions (Galerkin's method): $\boldsymbol{W}_n = \boldsymbol{J}^*_n$. This leads to N equations

$$V_m = \sum_{n=1}^{N} \iint_{S_m} Z_{mn} I_n, \qquad m = 1, 2, \ldots, N$$

which can be cast into the matrix form

$$\mathbf{V} = \mathbf{ZI} \tag{48}$$

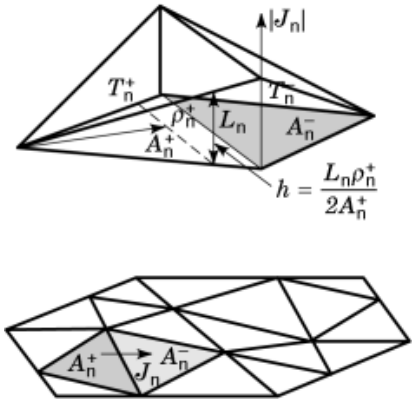

Fig. 14. Any arbitrary shaped surface can be represented by triangular facets. Triangular (rooftop) basis functions span each edge. The total current is a superposition of all of the basis functions at a point.

where

$$Z_{mn} = \iint_{S_m} \iint_{S_n} \left\{ j\omega\mu_0 \boldsymbol{W}_m(\boldsymbol{r}) \cdot \boldsymbol{J}_n(\boldsymbol{r}') - \frac{j}{\omega\epsilon} [\nabla' \cdot \boldsymbol{J}_n(\boldsymbol{r}')][\nabla' \cdot \boldsymbol{W}_m(\boldsymbol{r})] \right\} \times G(\boldsymbol{r}, \boldsymbol{r}')\, ds\, ds' \tag{49}$$

which is an impedance, and

$$V_m = \iint_{S_m} \boldsymbol{W}_m(\boldsymbol{r}) \cdot \boldsymbol{E}_i\, ds \tag{50}$$

which is a voltage. Thus Eq. (48) can be solved for **I**, then used in Eq. (47), which in turn is used in the radiation integrals to obtain the scattered field.

A commonly encountered basis function is the triangular subdomain (29). The surface of a target is represented by a collection of triangular facets. This type of subdomain has the flexibility to model curved surfaces with arbitrary edge contours. Each basis function is associated with an edge as shown in Fig. 14:

$$\boldsymbol{J}_n(\boldsymbol{r}') = \begin{cases} \dfrac{L_n \boldsymbol{\rho}_n^+}{2A_n^+}, & \boldsymbol{r}' \text{ in } T_n^+ \\ \dfrac{L_n \boldsymbol{\rho}_n}{2A_n^-}, & \boldsymbol{r}' \text{ in } T_n^- \end{cases} \tag{51}$$

The current at a point in a subdomain is the vector sum of the currents crossing all edges, weighted by the distance from the edge.

Using Eq. (51) in Eq. (49) gives

$$Z_{mn} = L_m \left(\frac{j\omega}{2} (\boldsymbol{A}_{mn}^{+} \cdot \boldsymbol{\rho}_m^{c+} + \boldsymbol{A}_{mn}^{-} \cdot \boldsymbol{\rho}_m^{c-}) + \Phi_{mn}^{-} - \Phi_{mn}^{+} \right)$$

where

$$\boldsymbol{A}_{mn}^{\pm} = \frac{\mu_0}{4\pi} \iint_{S_n} \boldsymbol{J}_n(\boldsymbol{r}') \frac{e^{-j\beta R_{mn}^{\pm}}}{R_{mn}^{\pm}} ds'$$

$$\Phi_{mn}^{\pm} = \frac{j}{4\pi\omega\epsilon_0} \iint_{S_n} \nabla' \cdot \boldsymbol{J}_n(\boldsymbol{r}') \frac{e^{-j\beta R_{mn}^{\pm}}}{R_{mn}^{\pm}} ds'$$

$$R_{mn}^{\pm} = |\boldsymbol{r}_{mn}^{c\pm} - \boldsymbol{r}'|$$

The excitation vector elements are

$$V_m = L_m (\boldsymbol{E}_m^{+} \cdot \boldsymbol{\rho}_m^{c+} + \boldsymbol{E}_m^{-} \cdot \boldsymbol{\rho}_m^{c-})$$

where the electric field at the centroid of the facet is

$$\boldsymbol{E}_m^{\pm} = \boldsymbol{E}_{\mathrm{i}}(\boldsymbol{r}_m^{c\pm})$$

These basis functions result in a linear approximation to the current over each facet. The rigorous result for the rectangular plate shown in Fig. 11 was computed using the method of moments.

There are a few instances when other basis functions may be more efficient than triangular subdomains. For example, consider a body of revolution (*BOR*), which is generated by rotating a plane curve around an axis. Included in this class are cylinders, cones, spheres, and ellipsoids. A hybrid basis function, that is, a combination of entire-domain and subdomain basis functions, is an efficient alternative to triangular facets (30). In these cases overlapping triangular basis functions can be used to represent the current along the generating curve axis, while entire-domain complex exponentials are used in the azimuthal direction (around the circumference of the body). The result is a linear approximation to the current in the axial direction (from back to front) and a Fourier series representation for the current around the body. The major advantage of this approach is that each Fourier mode, which is actually a matrix whose size is determined by the number of subdomains along the axis, is independent of all other modes. Thus a large-matrix problem is decomposed into a series of smaller matrices, thereby permitting larger bodies to be modeled for a given computer resource.

Hybrid Methods. Hybrid computation methods combine several prediction techniques in a single solution (31,32). A hybrid solution decomposes a problem into subproblems, which are solved using different techniques. Generally the mutual effects (interaction between the subproblems) are included to some degree. For example, PO is known to give excellent results for large smooth surfaces away from edges and discontinuities. A hybrid approach might use PO on regions of the surface away from discontinuities and the MM near discontinuities. Larger problems can modeled than with a pure MM approach, and more accuracy is achieved than using PO separately. The disadvantage is that each hybrid combination is tailored for a specific type of problem and therefore may not yield accurate results under all conditions.

One hybrid method that is used extensively in RCS calculation for large targets at high frequencies is the shooting and bouncing ray (SBR) technique (33). It combines GO and PO, and can be supplemented by

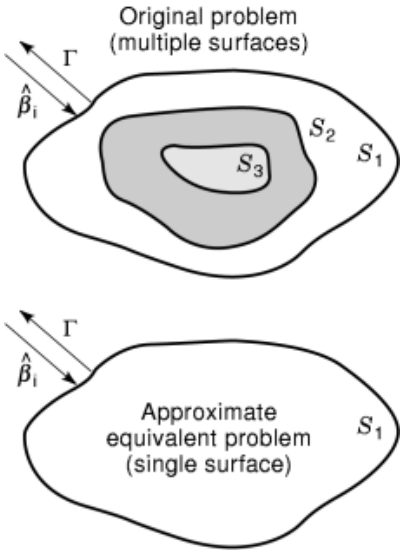

Fig. 15. A complex multilayered target can be replaced by an equivalent target having the same surface contour but an equivalent surface impedance.

the PTD. Current distributions are determined from the trajectories of rays in a dense bundle. The current distributions can be used to:

(1) Initiate secondary rays to evaluate multiple reflections
(2) Compute PTD fringe currents for edge diffraction contributions
(3) Compute the far scattered fields

Currently this technique is the most accurate and flexible for computing the RCSs of large complex targets such as aircraft with engine inlets and cockpits.

Surface Impedance Approximation. The *impedance boundary* is an approximate boundary condition that can be used to replace a surface composed of multiple materials and layers by a single surface. It was first proposed by Leontovich (34) and is frequently referred to as the Leontovich boundary condition. The concept is illustrated in Fig. 15, which shows the use of a surface current approach to calculate the scattered field from a target composed of several materials.

The possibility of surface currents flowing on all of the interfaces dramatically increases the mathematical and computational complexity of the problem over that of a single surface. In many cases it may be sufficient to replace the collection of surfaces with a single layer that has approximately the same external scattering properties as the combination of original surfaces. (For the RCS the fields inside the body are not of interest.) The same scattering properties for the original and equivalent problems are ensured if the boundary conditions on the tangential field components are the same. The required relationship between the electric and magnetic fields is referred to as a *surface impedance approximation.*

Mathematically it relates the tangential components of the electric and magnetic fields at every point on the surface:

$$\eta_{/s} = \frac{|\boldsymbol{E}_{\tan}|}{|\boldsymbol{H}_{\tan}|} \tag{52}$$

where η_s is the surface impedance in ohms. In vector form,

$$\eta_s \hat{\boldsymbol{n}} \times \boldsymbol{H} = \boldsymbol{E} - (\hat{\boldsymbol{n}} \cdot \boldsymbol{E})\hat{\boldsymbol{n}} = \eta_s \boldsymbol{J}_s \tag{53}$$

There is a dual to this equation:

$$-\frac{1}{\eta_s}\hat{\boldsymbol{n}} \times \boldsymbol{E} = \boldsymbol{H} - (\hat{\boldsymbol{n}} \cdot \boldsymbol{H})\hat{\boldsymbol{n}} = \frac{1}{\eta_s}\boldsymbol{M}_s \tag{54}$$

Comparing Eqs. (53) and (54) reveals that the surface impedance relates the electric and magnetic currents at every point on the surface:

$$\boldsymbol{M}_s = -\eta_s \hat{\boldsymbol{n}} \times \boldsymbol{J}_s \tag{55}$$

Note that $\eta_s = 0$ corresponds to a PEC, and the resulting reflection coefficient for a wave normally incident on the PEC is

$$\Gamma = \frac{\eta_s - \eta_0}{\eta_s + \eta_0} = -1 \tag{56}$$

The surface impedance approximation is most accurate when:

(1) The surface is electrically large and the incident wave is near normal incidence to the surface ($\theta_i \approx 0^\circ$).
(2) The relative dielectric constant of the material is high ($\sqrt{\epsilon_r} \gg 1$).
(3) The local radius of curvature of the surface is large compared to a wavelength.

Impedance boundary conditions can be used to derive integral equations (35) or to simplify an approximate solution. They are widely used in spite of the fact that they usually cannot be justified rigorously.

An estimate of the surface impedance can be obtained from the permittivities and permeabilities of the constituent materials. For layers, a transmission line model can be used to compute the reflection coefficient at the outer surface, and then Eq. (56) solved for η_s. Using this approach, η_s is a function of the angle of incidence because the Fresnel reflection coefficients are angle-dependent. Generally an average value near normal incidence is used, because it is near the local normal that each region of the surface makes its greatest contribution to the RCS.

A second set of approximate boundary conditions are used to represent thin films (36). They are the resistive sheet and conductive sheet boundary conditions, which provide a relationship between the currents on the surface and the tangential field components. A resistive sheet is an infinitely thin imperfect electric conductor (finite conductivity) and it does not support a magnetic current:

$$\boldsymbol{E}_{\tan} = \boldsymbol{J}_s R_s \tag{57}$$

where R_s is the surface resistivity in ohms per square. The limiting cases are $R_s = 0$ for a PEC and $R_s = \infty$ for a perfectly transparent sheet. The reflection coefficient of the sheet is

$$\Gamma = \frac{-\eta_0}{2R_s + \eta_0} \tag{58}$$

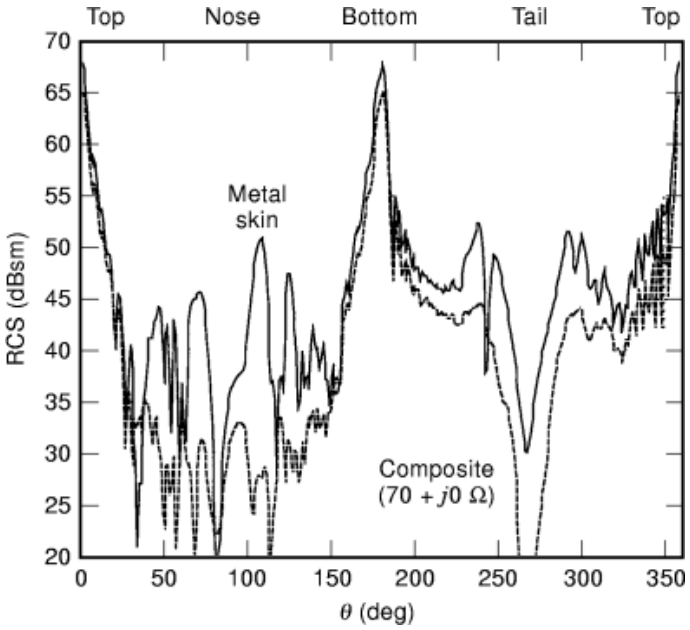

Fig. 16. The RCS of a metal skin aircraft is compared to that of a composite aircraft. The monostatic RCS is lower for the composite aircraft because more of the incident field is scattered in the forward direction. The surface impedance approximation has been used.

Resistive films are an effective means of controlling the reflection coefficient of a surface. They consist of thin metallic deposits on low-dielectric films such as *Mylar*. A common example of a commercially available resistive film is window tinting of the type used for automobiles.

The dual of the resistive sheet is the *conductive sheet,* with the boundary condition

$$\boldsymbol{M}_s = -\frac{\boldsymbol{H}_{\tan}}{G_s} \tag{59}$$

where G_s is the surface conductance. The conductive sheet does not support an electric current. A combination of resistive and conductive sheets can be viewed as an *impedance sheet.*

Figure 16 compares the RCSs of PEC and composite aircraft wings. The RCS of the composite wing is significantly reduced because more of the wave is transmitted and less reflected.

Rough Surfaces. Imperfections and errors in the assembly and manufacturing processes have a significant effect on the low-level RCS. The sources of errors are variations in the physical dimensions and electrical characteristics of the target materials. Most of the errors behave in a random fashion. Random deviations in the characteristics of a target result in an increase in diffuse scattering and a corresponding decrease in specular reflection.

The Rayleigh condition is the traditional criterion for a rough surface:

$$\overline{h} \leq \frac{\lambda}{8 \sin \psi}$$

where $\bar{h}$ is the average height of the irregularities and $\psi$the grazing angle. The surface impedance boundary condition can also be used to simulate surface irregularities (37).

The calculation of the RCS for targets with random characteristics can be performed using a Monte Carlo simulation (method of repeated trials) or by applying probability theory to the governing equations of electromagnetics. Both approaches start by writing the RCS in terms of the random variables of interest (for example, target dimensions). In the Monte Carlo method, the equations are computer-programmed and repeatedly executed using a different random seed each time. The average RCS and its standard deviation can be computed from the output data.

Another approach is to take the expected value of the RCS expression. If the probability density functions of the random variables are known, then the expectation operation results in an expression for the average RCS. Using this approach, the RCS of a "lumpy" surface with a correlation interval $\bar{c}$ (the distance beyond which on average the surface deviations become independent) is given approximately by (6)

$$\sigma = \frac{4\pi A^2}{\lambda^2}\cos^2\theta\, e^{-4\beta^2\overline{\delta^2}}\left[P_0 + \frac{4\pi\bar{c}^2\beta^2\overline{\delta^2}}{A}\exp\left(\frac{c^2\pi^2\sin^2\theta}{\lambda^2}\right)\right] \tag{60}$$

where$\sqrt{\delta^2}$ is the variance of the surface deviations (assumed small). P_0 is the error-free power pattern normalized to A^2. (Using a flat plate as an example, $P_0 = [\mathrm{sinc}(\beta u a)\ \mathrm{sinc}(\beta v b)\cos\theta]^2$.) The second term in the brackets of Eq. (60) represents a random noise that increases with the level of the error. A small correlation interval yields lower, more uniformly dispersed scattering than a large correlation interval.

Measurement of Radar Cross Section

Measurements are a crucial step in the design and verification of an LO platform. In general, measured RCS data can serve three purposes:

(1) To establish a target's RCS for design verification
(2) For comparison with calculated RCS to evaluate numerical methods or the validity of approximations
(3) As a diagnostic tool

Measurements are performed throughout the design of a stealthy platform. During the conceptual stage, scale models of candidate designs may be built and tested to verify that the RCS levels are close to those expected. At various stages in the development of the full-scale components (such as wings and antennas), measurements can be used to verify assembly tolerances, RCS treatments, and other manufacturing processes. Problem areas can be reworked and then checked again. Finally, if the target is not too large, a measurement can be made on the completed product. This step may serve as part of the official fulfillment of a contract.

Measurement facilities can be categorized by a variety of attributes that include physical characteristics, instrumentation capabilities, and data analysis and presentation modes. Table 4 summarizes some commonly used descriptors.

Most systems measure monostatic RCSs by using a fixed transmit/receive antenna and rotating the target. The traditional continuous wave (*CW*) measurement involves two steps. First, a calibration target of known RCS (typically a sphere) is placed in the chamber, and the received power is recorded for reference. Next, the calibration target is replaced by the object with unknown RCS, and the power measured as the target is rotated. By comparing the received and reference powers, the RCS of the unknown target is obtained. In an analog system, the power difference drives the vertical (RCS) axis of a plotter, and the horizontal (angle) axis

Table 4. RCS Measurement Facility Descriptors

System Descriptor	Categories
Physical Configuration	Indoor/outdoor
	Near field
	Far field
	Compact
	Tapered
Instrumentation	Time domain
	Frequency domain
	Continuous wave (CW)
	Pulsed CW
Data analysis and presentation	Fixed frequency/variable aspect
	Fixed aspect/frequency sweep
	Two-dimensional frequency
	Aspect
	Time domain trace
	Target imaging
	Polar or rectangular plots

is slewed to the target mount. The final result is a plot of RCS versus aspect angle. The data obtained using the classical far-field CW RCS measurement of a rectangular plate are illustrated in Fig. 17.

For a true far-field measurement the target must be illuminated by a plane wave. This condition is never rigorously satisfied in practice, because the need for a directive transmit antenna usually results in a nonuniform-amplitude illumination of the target. Furthermore, the wave incident on the target is always spherical, not planar. Finally, because the system components are near the floor, ceiling, and walls, reflections from these surfaces affect the measurement.

Figure 17 illustrates the types of inaccuracies that can occur, such as sidelobe asymmetry and the existence of a noise floor. The noise floor sets a lower limit on the RCS that can be reliably measured. Measures of chamber performance are:

(1) Pattern symmetry in angle
(2) Noise floor (noise level)
(3) Quiet zone (linear extent of the region where the amplitude and phase of the incident wave are approximately plane)
(4) Repeatability
(5) Allowable target size and weight for the mount
(6) Allowable range of target motion
(7) Instrumentation capabilities
(8) Data-processing capabilities
(9) Data-presentation capabilities

The state-of-the-art instrumentation used in RCS measurement is essentially a programmable multimode radar. Data can be collected in either the time or the frequency domain and transformed back and forth between the two. In the time domain, gating can be employed to discard signals that do not correspond to the time delay of a scattered signal from the target's extent. Processing such as *windowing* can be performed on the raw

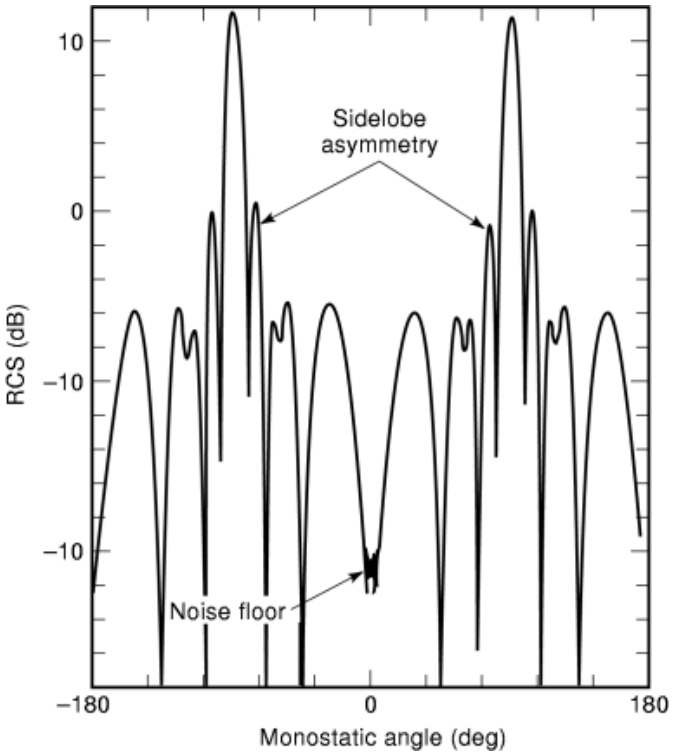

Fig. 17. The measured RCS of a 16 inch square plate for a 2 GHz CW source. Errors in the measurement were more pronounced in older measurement systems. Background subtraction techniques can be used to reduce measurement errors.

data to enhance various characteristics and then see how they behave as a function of frequency or aspect. Data-processing techniques can even generate high-resolution images that highlight scattering hot spots on the target.

Chamber Configurations. The majority of all RCS measurement facilities are completely enclosed (indoor ranges). This provides isolation from the external environment, which is desirable for both security and technical reasons. In an indoor chamber the interference from other RF sources is reduced or eliminated, and the temperature is controlled for increased instrumentation stability. The result is a more accurate and repeatable measurement than possible in an outdoor facility. The obvious limitation on an indoor chamber is the size of the building required for large targets.

Figure 18 shows two types of indoor chambers. The first is the standard far-field configuration. The separation of the antenna and target must be large enough so that the difference between an ideal plane wave and the actual spherical wave is negligible. The required distance is a function of target size and the frequency. If the distance is R and the target length L, as indicated in Fig. 19, the round trip phase difference between rays to the edge and center is

$$2\beta\Delta_{\max} = 2\beta[\sqrt{R^2 + (L/2)^2} - R] \approx \frac{\pi L^2}{2R\lambda} \qquad (61)$$

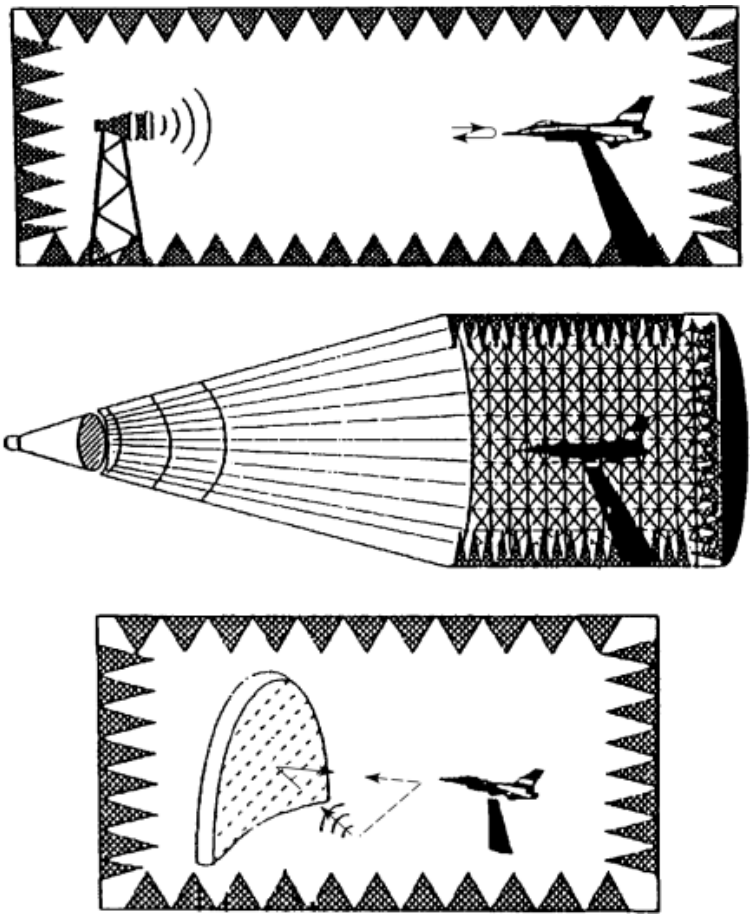

Fig. 18. Common indoor chamber configurations include the conventional far-field range, the tapered chamber, and the compact range. The compact range is capable of handling physically large targets over a wide frequency range.

where the right-hand side holds for $R \gg L$. Based on the convention used for the definition of the far field of a radiating antenna, one may limit the round trip phase error to $\pi/8$, so that the minimum range becomes

$$R_{\min} = \frac{4L^2}{\lambda}$$

This limit turns out to be overly restrictive and is usually not adhered to in practice. Equation (61) assumes that all of the target surface contributes coherently to the total RCS, as will happen for example, with a smooth plate. On the other hand, if the target is composed of many independent scatterers, the far-field distance is primarily determined by the distribution of dominant scatterers in space. Thus when the dominant scatterers are clustered, a much smaller range is acceptable (38).

In addition to a plane phase front at the target, the amplitude of the incident wave across the target must be constant. The amplitude distribution is controlled by the antenna beamwidth and the ratio L/R. An isotropic antenna provides the flattest phase front, but also results in stronger illumination of the chamber walls and

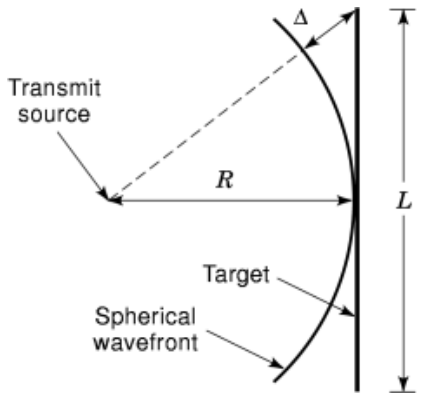

Fig. 19. The incident spherical wave from the transmitter deviates from a plane wave. The deviation leads to an error in the measured RCS. To reduce the error the transmitter to target distance must be increased.

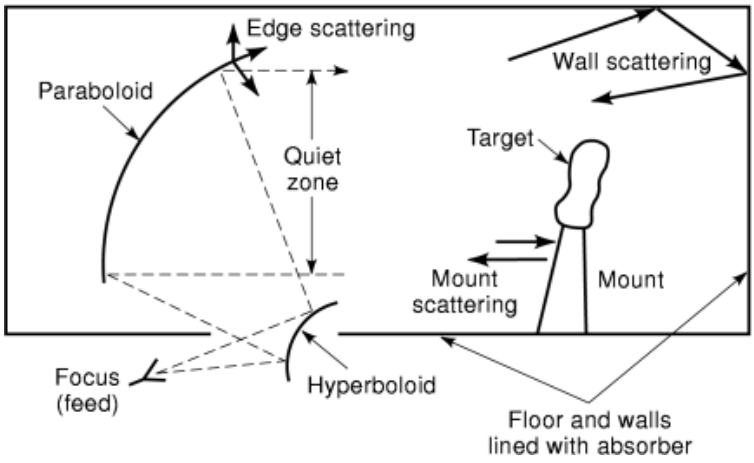

Fig. 20. A compact range provides a uniform field over the target with shorter antenna-to-target distances than a conventional far-field range. Some sources of measurement error are illustrated.

other obstacles. The transmitted power must also be higher if the antenna gain is low. Thus there is a tradeoff involved in determining the optimum antenna configuration.

The demands on chamber size required for accurate low-level RCS measurements have resulted in the development of *compact ranges.* The layout of a typical compact range is shown in Fig. 20. The parent reflector configuration is a Cassegrain, and the reflector surfaces have been arranged so that no blockage occurs. The antenna is located at the focus, and a plane wave field is excited a short distance in front of the paraboloid. The total volume of a compact range is much less than that of a far-field configuration.

The compact range is not without its own problems, though. To obtain uniform amplitude over the target requires a shaped feed pattern or some subreflector shaping. Cross polarization and edge diffraction can be significant. Since the target is close to the reflector edges, the effects of edge scattering are especially important at low RCS levels. Much effort has gone into the design of rolled or serrated edges that control the level and direction of edge diffraction.

Sources of Measurement Error. The received signal in a measurement is not entirely due to scattering from the target. It also includes noise introduced by the receiving system and extraneous scattered signals

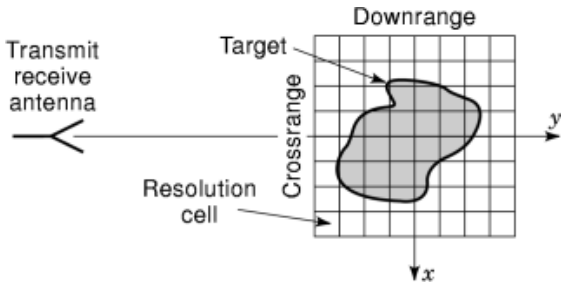

Fig. 21. Radar images can be generated by plotting the intensity of the scattered field as a function of the target surface coordinates. The downrange size of the resolution cell is determined by the radar pulsewidth; the crossrange resolution is determined by the Doppler measurement capability of the radar.

originating from the chamber walls and other obstacles. Furthermore, some of the transmit signal couples directly to the receive antenna. This leakage is strongest when a common antenna is used for both transmit and receive.

Chambers that are used to measure low-level RCSs must be carefully designed, maintained, and calibrated. Great care is taken to reduce the error signals in the vicinity of the target. The cross-sectional dimension of the chamber that is essentially free of extraneous signals and maintains the plane wave phase and amplitude is called the *quiet zone.* It is usually specified in feet or meters. The quiet zone, frequency range of operation, and noise floor effectively characterize the chamber performance.

Measurement errors are mitigated using background subtraction. First a measurement is taken with the target absent. Ideally the received signal should be zero if the chamber walls are perfect absorbers and there is no leakage. In practice a nonzero signal is present due to the sources indicated in Fig. 20, and this value is stored as a reference. Next, the measurement is repeated with the target present. The measured value includes the target's RCS as well as the error signals. If the interaction between the target and chamber is negligible, vector subtraction of the background signal should yield a close approximation to the isolated target's RCS.

The subtraction method requires that the characteristics of the measurement equipment remain stable during the calibration and measurement runs. If the power level or frequency drifts, the background reference is no longer valid and the difference is attributed to the target. Even small changes in phase caused by cable movement can affect low RCS measurements.

Target Mounts. A potential source of large measurement error is the target mount. If at all possible, the pedestal should be made of low-density material that does not scatter. Frequently the target is suspended and held in tension using thin polyester filaments similar to fishing line. For large, heavy targets that must be tilted and rotated there is no alternative but to use metal mounts. In this case special shaped fixtures are used to shield the pedestal. Absorbing material can also be used in conjunction with shaping to reduce mount scattering.

Resolved RCS and Target Imaging. Returns from individual scattering elements on a complex target can be isolated or resolved. The strength of the return is plotted as a function of downrange (y) and crossrange (x) in Fig. 21. If the cell size becomes small enough, a high-resolution two-dimensional image of the target can be constructed. As shown in Fig. 22, imaging clearly identifies the strongest scattering sources on a target.

Resolving the individual scattering sources on a target requires that accurate angle and range information be available as the returns are received. Range resolution is achieved by using a short pulse that only illuminates a small slice of the target. Knowledge of the time elapsed after the leading edge of the pulse hits the target is equivalent to knowledge of the downrange coordinate y.

One method of obtaining the crossrange value is by accurately pointing a narrow antenna beam. The beam is scanned over the entire solid angle of the target, thereby providing angle data that can be processed

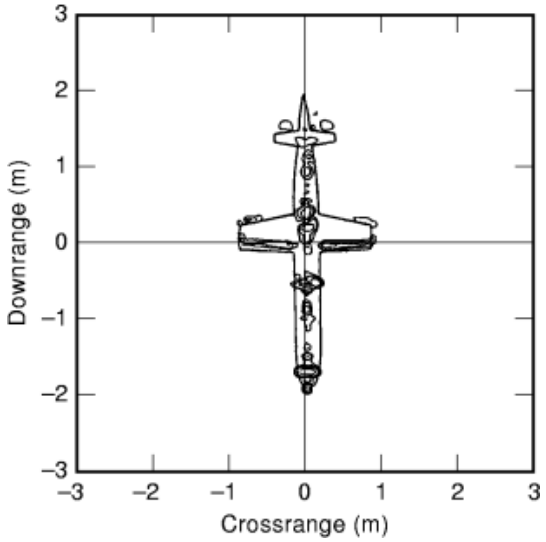

Fig. 22. The radar image of the target can be used to determine where RCS treatments should be applied, as well as evaluate the effectiveness of RCS reduction methods.

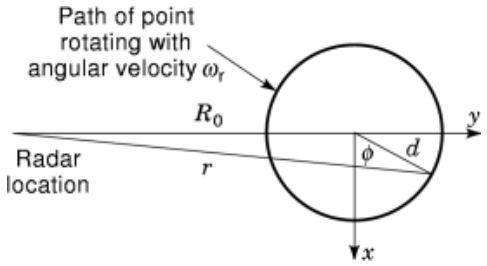

Fig. 23. A point rotating on the surface of the target has a Doppler frequency shift. The frequency shift can be used to determine the crossrange coordinate.

along with the range data to construct an image. This approach is not efficient at microwave frequencies, however, because of the large antenna size needed for fine angle resolution. It is more practical at millimeter wavelengths and smaller, and is highly successful at laser wavelengths. A more practical method for obtaining crossrange exploits the Doppler shift (39). The target is rotated at an angular velocity ω_r as shown in Fig. 23. Target surface points rotate with a linear velocity that depends on their distance from the center of rotation. The radial component of relative velocity (component along R) gives rise to a Doppler shift.

Referring to the coordinate system shown in Fig. 23, let R_0 be the range to the target's center of rotation along the y coordinate, and r the distance to a scattering point at a distance d from the center. Using the law of cosines,

$$r^2 = R_0^2 + d^2 - 2dR_0 \cos\phi$$

which simplifies to

$$r = R_0\sqrt{1 - \frac{2d\sin\phi}{R_0}}$$

when $R_0 \gg d$. The first term under the square root is associated with the round trip time delay to and from the target center, and the second is the Doppler shift due to rotation. Since $\phi = \omega_r t$ (where ω_r is the rotation rate of the target), the Doppler frequency in hertz is

$$f_d = \frac{1}{2\pi}\frac{d}{dt}(-2\beta R_0 + 2\beta d\sin\omega t) = \frac{2\omega_r}{\lambda}x \qquad (62)$$

This method of rotating the target to obtain crossrange information is the same principle used in inverse synthetic aperture radar (ISAR) method.

BIBLIOGRAPHY

1. M. Skolnik, *Introduction to Radar Systems*, 2nd ed., New York: McGraw-Hill, 1980.
2. B. Eddie, *Radars*, Engelwood Cliffs, NJ: Prentice-Hall, 1993.
3. G. Ruck *et al.*, *Radar Cross Section Handbook*, New York: Plenum, 1970.
4. C. Balanis, *Advanced Engineering Electromagnetics*, San Francisco: Harper & Row, 1982.
5. K. Kunz, R. Luebbers, *The Finite-Difference Time Domain Method for Electromagnetics*, Boca Raton, FL: CRC Press, 1993.
6. D. Jenn, *Radar and Laser Cross Section Engineering*, Washington, DC: AIAA Education Series, 1995.
7. A. Ishimaru, *Electromagnetic Wave Propagation and Scattering*, Englewood Cliffs, NJ: Prentice-Hall, 1991.
8. L. Peters, End-fire echo area of long, thin bodies, *IRE Trans. Antennas Propag.*, 133, January 1958.
9. R. Harrington, *Time-Harmonic Electromagnetic Fields*, New York: McGraw-Hill, 1961.
10. J. Keller, Determination of reflected and transmitted fields by geometrical optics, *J. Opt. Soc. Amer.*, **40** (1): 48, 1950.
11. R. Harrington, *Field Computation by Moment Methods*, New York: Macmillan, 1961.
12. W. Streetman, J. Goodall, *Lockheed F-117A*, Osceola, WI: Motorbooks International, 1990.
13. D. Cheng, *Field and Wave Electromagnetics*, 2nd ed., New York: McGraw-Hill, 1989.
14. M. Schwartz, *Composite Materials Handbook*, 2nd ed., New York: McGraw-Hill, 1992.
15. V. Weston, Theory of absorbers in scattering, *IEEE Trans. Antennas Propag.*, **AP-11**: 578, 1963.
16. N. Engheta, D. Jaggard, Electromagnetic chirality and its applications, *IEEE Antennas Propag. Soc. Newslett.*, 6, October 1968.
17. R. Harrington, Theory of loaded scatterers, *Proc. IEE Electron.*, **111** (4): 617–623, 1964.
18. R. Harrington, The control of electromagnetic scattering by impedance loading, *Proc. IEEE*, **53**: 993–1004, 1965.
19. E. Knott, J. Schaeffer, M. Tuley, *Radar Cross Section*, Norwood, MA: Artech House, 1989.
20. *Navy Times*, Jan. 12, 1998, p. 4.
21. E. Pelton, B. Munk, A streamlined metallic radome, *IEEE Trans. Antennas Propag.*, **AP-22**: 799, 1974.
22. D. C. Schleher, *Introduction to Electronic Warfare*, Norwood, MA: Artech House, 1986.
23. S. Silver, *Microwave Antenna Theory and Design*, New York: McGraw-Hill, 1949.
24. P. Ufimtsev, *Method of Edge Waves in the Physical Theory of Diffraction*, translated from Russian by the USAF Systems Command, Foreign Technology Division, Sept. 7, 1971.
25. A. Michaeli, Equivalent edge currents for arbitrary aspects of observation, *IEEE Trans. Antennas Propag.*, **AP-32**: 252–258, 1984; corrections, **AP-33** (2), 1985.
26. J. Keller, Geometrical theory of diffraction, *J. Opt. Soc. Amer.*, **52** (2): 116, 1962.
27. R. Kouyoumjian, P. Pathak, A uniform geometrical theory of diffraction for an edge in a perfectly conducting surface, *Proc. IEEE*, **62**: 1448, 1974.

28. J. Boersma, Y. Rahmat-Samii, Comparison of two leading theories of edge diffraction with the exact uniform asymptotic solution, *Radio Sci.*, **15** (6): 1179, 1980.
29. S. Rao, D. Wilton, A. Glisson, Electromagnetic scattering by surfaces of arbitrary shape, *IEEE Trans. Antennas Propag.*, **AP-30**: 409, 1982.
30. L. Medgyesi-Mitschang, J. Putnam, Hybrid solutions for scattering from large bodies of revolution with material discontinuities and coatings, *IEEE Trans. Antennas Propag.* **AP-32**: 717, 1984.
31. E. Ekelman, G. Thiele, A hybrid technique for combining the moment method treatment of wire antennas with the GTD for curved surfaces, *IEEE Trans. Antennas Propag.*, **AP-28**: 831, 1980.
32. T. J. Kim, G. Thiele, A hybrid diffraction technique—general theory and applications, *IEEE Trans. Antennas Propag.*, **AP-30**: 888–898, 1982.
33. H. Ling, R. Chou, S. Lee, Shooting and bouncing rays: Calculating the RCS of an arbitrarily shaped cavity, *IEEE Trans. Antennas Propag.*, **AP-37**: 194, 1989.
34. T. Senior, Impedance boundary conditions for imperfectly conducting surfaces, *Appl. Sci. Res.*, **8(B)**: 418, 1960.
35. L. Medgyesi-Mitschang, J. Putnam, Integral equation formulations for imperfectly conducting scatterers, *IEEE Trans. Antennas Propag.*, **AP-33**: 206, 1985.
36. T. Senior, Combined resistive and conductive sheets, *IEEE Trans. Antennas Propag.*, **AP-33**: 577, 1985.
37. T. Senior, Impedance boundary conditions for statistically rough surfaces, *Appl. Sci. Res.*, **8(B)**: 437, 1960.
38. B. Welsh, A minimum range criterion for RCS measurements of a target dominated by point scatterers, *1984 AP-S/URSI Int. Symp.*, Vol. APS-17-3, p. 666, 1984.
39. D. Mensa, *High Resolution Radar Cross Section Imaging*, Norwood, MA: Artech House, 1981.
40. *RCS Measurement Capabilities at the Pacific Missile Test Center*, Pt. Mugu, CA: Radar Signature Branch.

DAVID C. JENN
Naval Postgraduate School